Efficient and multiplexed somatic genome editing with Cas12a mice

Jess D. Hebert[1], Haiqing Xu[3], Yuning J. Tang[1], Paloma A. Ruiz[1], Colin R. Detrick[1], Jing Wang[2], Nicholas W. Hughes[1], Oscar Donosa[1,5], Laura Andrejka[1], Saswati Karmakar[1], Irenosen Aboiralor[1], Rui Tang[1], Julien Sage[1,5], Le Cong[1,6], Dmitri A. Petrov[3,4,7], and Monte M. Winslow[1,4,6#]

[1] Department of Genetics, Stanford University School of Medicine, Stanford, CA, USA
[2] Department of Radiology, Stanford University School of Medicine, Stanford, CA, USA
[3] Department of Biology, Stanford University, Stanford, CA, USA
[4] Cancer Biology Program, Stanford University School of Medicine, Stanford, CA, USA
[5] Department of Pediatrics, Stanford University School of Medicine, Stanford, CA, USA
[6] Department of Pathology, Stanford University School of Medicine, Stanford, CA, USA
[7] Chan Zuckerberg Biohub Investigator

[#] Corresponding author:

Monte M. Winslow, Stanford University School of Medicine | 279 Campus Drive, Beckman Center B256, Stanford, CA 94305 | Phone: 650-725-8696 | Fax: 650-725-1534 | E-mail: mwinslow@stanford.edu

ABSTRACT

Somatic genome editing in mouse models has increased our understanding of the *in vivo* effects of genetic alterations in areas ranging from neuroscience to cancer biology and beyond. However, existing models are limited in their ability to create multiple targeted edits. Thus, our understanding of the complex genetic interactions that underlie development, homeostasis, and disease remains incomplete. Cas12a is an RNA-guided endonuclease with unique attributes that enable simple targeting of multiple genes with crRNA arrays containing tandem guides. To accelerate and expand the generation of complex genotypes in somatic cells, we generated transgenic mice with Cre-regulated and constitutive expression of enhanced *Acidaminococcus sp.* Cas12a (enAsCas12a). In these mice, enAsCas12a-mediated somatic genome editing robustly generated compound genotypes, as exemplified by the initiation of diverse cancer types driven by homozygous inactivation of trios of tumor suppressor genes. We further integrated these modular crRNA arrays with clonal barcoding to quantify the size and number of tumors with each array, as well as the efficiency of each crRNA. These Cas12a alleles will enable the rapid generation of disease models and broadly facilitate the high-throughput investigation of coincident genomic alterations in somatic cells *in vivo*.

INTRODUCTION

Genetically engineered mouse models have been widely used to uncover phenotypes resulting from defined genetic alterations[1]. However, the creation of new mouse alleles has remained a barrier to the study of more complex genotypes, due to the expense and time required to generate a new allele and cross it with other alleles of interest[2]. Somatic genome editing with

57 Cas9 has greatly increased the rate at which single genes can be studied both *ex vivo* and *in vivo*,
58 but the ability of Cas9 to model complex genotypes has been limited by the need for each guide to
59 have its own promoter and tracrRNA, thereby requiring the laborious cloning of guides in
60 sequence[3].

61 Cas12a (previously known as Cpf1) is a Class 2 Type V CRISPR-Cas system that has
62 unique value in genome editing due to its ability to easily target multiple genomic loci[4–6]. Unlike
63 Cas9, Cas12a has both RNase and DNase activity, and can process a single pre-crRNA transcript
64 (crRNA array) containing numerous spacers (guides) into its constituent crRNAs to direct Cas12a-
65 mediated cleavage of their target regions[4]. Cas12a is also distinct from Cas9 in recognizing a T-
66 rich 4 bp protospacer adjacent motif (PAM) and generating staggered cuts that are distal to the
67 PAM[5]. Cas12a from multiple species has been employed for genome editing *in vitro*, including
68 Cas12a from *Acidaminococcus sp.* (As) and *Lachnospiraceae bacterium* (Lb)[4,6–11]. Large-scale
69 screens have identified Cas12a variants with increased efficiency, broadened PAM recognition
70 ranges, and reduced off-target cleavage[12–15]. In particular, an enhanced version of AsCas12a
71 (enAsCas12a) with several substitutions (E174R/N282A/S542R/K548R) has superior genome
72 editing relative to wild type AsCas12a, in addition to a substantially expanded targeting range[13].

73 The impact of complex genotypes is highly relevant in human cancer, which is defined by
74 its genetic complexity. Individual tumors can have tens to hundreds of non-synonymous mutations,
75 in addition to aberrant epigenetic modifications, gene duplications, chromosomal rearrangements,
76 and gains or losses of entire chromosomes[16–18]. Any or all of these alterations could contribute to
77 tumorigenesis, tumor progression, and resistance to therapy. Deconvoluting functional drivers
78 from human cancer sequencing data and understanding how these genes interact to generate cancer
79 phenotypes is complicated by the limited availability of samples, differences among patients and

80 which therapies they have received, and technical variability of the approaches used to analyze
81 them. Functional interrogation of the phenotypes resulting from defined combinations of
82 alterations is thus critical for isolating the key drivers of these complex disease states.

83 To accelerate and expand our ability to generate complex genotypes in somatic cells, we
84 generated Cre-regulated and constitutive enAsCas12a transgenic mice. Efficiently multiplexed
85 somatic genome editing using Cas12a transgenic mice enables the rapid generation of complex
86 models and should facilitate the high-throughput investigation of coincident genomic alterations
87 *in vivo*.

88

89 **RESULTS**

90

91 **Generation and validation of Cre-regulated and constitutive enAsCas12a alleles**

92 To enable Cas12a-mediated somatic genomic editing and thus take advantage of the
93 features that distinguish Cas12a from Cas9 (**Supplementary Figure 1a**), we generated transgenic
94 mice expressing enAsCas12a with an optimized nuclear localization sequence (NLS)
95 configuration that increases cutting efficiency and an HA tag to facilitate identification
96 (enAsCas12a; **Figure 1a**)[13,19]. We generated transgenic mice through integration of a CAGGS
97 promoter-driven Lox-Stop-Lox (LSL)-enAsCas12a-PolyA cassette into the *H11* locus ($H11^{LSL-}$
98 ^{Cas12a}) (**Figure 1a,b**). Expression of Cre in fibroblasts from $H11^{LSL-Cas12a}$ mice induced
99 recombination of the LSL cassette and expression of Cas12a protein (**Figure 1c**). We also crossed
100 $H11^{LSL-Cas12a}$ mice to CMV-Cre "deleter" mice to generate a constitutive $H11^{Cas12a}$ allele (**Figure**
101 **1d** and **Supplementary Figure 1b**). $H11^{Cas12a}$ mice were viable and fertile and had widespread

102 expression of Cas12a (**Figure 1e**), with prominently nuclear protein localization (**Figure 1f** and
103 **Supplementary Figure 1c**).
104
105 **Cas12a-induced inactivation of *Nf1, Rasa1* and *Pten* generate lung adenocarcinoma**
106 Oncogene-negative lung adenocarcinoma represents ~30% of all lung adenocarcinomas
107 and has been modeled in mice through combinatorial inactivation of the tumor suppressor genes
108 *Nf1*, *Rasa1* and *Pten* in lung epithelial cells[20]. This was initially accomplished using Cas9-
109 mediated somatic genome editing and multi-step sgRNA cloning[20]. As an initial test of the ability
110 of the $H11^{LSL\text{-}Cas12a}$ allele to generate tumors with complex genotypes *in vivo*, we generated
111 lentiviral vectors expressing Cre and a pre-crRNA array targeting *Nf1*, *Rasa1*, and *Pten*. Given the
112 ability to synthesize these three-crRNA arrays and their ease of cloning, we generated a pool of 27
113 lentiviral Cre vectors with every combination of three guides targeting each tumor suppressor gene
114 (**Figure 2a**). We cloned these pre-crRNA arrays into a vector that contained a diverse 16-
115 nucleotide barcode (BC) at the 3' end of the U6 promoter and Cre recombinase (Lenti-$U6^{BC}$-
116 cr*Nf1/Rasa1/Pten*-Cre; **Figure 2b**). Cre in these vectors induces Cas12a expression in somatic
117 cells in $H11^{LSL\text{-}Cas12a}$ mice, and amplification of the BC-crRNA region from bulk tumor-bearing
118 lungs followed by tumor barcoding and high-throughput barcode sequencing (Tuba-seq^{Ultra}; U6
119 barcode Labeling with per-Tumor Resolution Analysis) can quantify the size of each clonal
120 tumor[21–23].
121 We transduced the lungs of $H11^{LSL\text{-}Cas12a}$ mice (some of which also contained a $R26^{LSL\text{-}}$
122 ^{Tomato} Cre-reporter allele), wild-type negative control mice, and $Kras^{LSL\text{-}G12D}$;$R26^{LSL\text{-}Tomato}$ (*KT*)
123 positive control mice with Lenti-$U6^{BC}$-cr*Nf1/Rasa1/Pten*-Cre (**Figure 2c**). Tumors in *KT* mice
124 form due to Cre-mediated expression of oncogenic KRAS in the absence of any Cas12a-mediated

125 gene targeting. We anticipated that Cas12a-mediated homozygous inactivation of *Nf1, Rasa1,* and
126 *Pten* might be limited; therefore, we used a 5-fold higher titer in *H11*$^{LSL\text{-}Cas12a}$ mice relative to *KT*
127 mice in which every transduced cell will express oncogenic KRAS. Unexpectedly, only 9 weeks
128 after tumor initiation, the *H11*$^{LSL\text{-}Cas12a}$ mice developed extremely high tumor burden as assessed
129 by lung weight (>15-folder higher than *KT* mice after subtracting normal lung weight), direct
130 imaging of the lung lobes, and histology (**Figure 2 d-f**). Histology, positive immunohistochemical
131 staining for NKX2-1/TTF-1, and negative staining for UCHL1 confirmed that these tumors were
132 lung adenomas and adenocarcinomas (**Figure 2f**)[20]. Neoplastic cells in these tumors expressed
133 nuclear Cas12a (**Supplementary Figure 2g**). PCR amplification and Sanger sequencing of each
134 of the 9 targeted regions from genomic DNA from bulk tumor-bearing lungs from *H11*$^{LSL\text{-}Cas12a}$
135 mice confirmed indels at each target site (**Figure 2h**).
136

137 **Quantification of Cas12a-mediated tumorigenesis**

138 We PCR-amplified and high-throughput sequenced the BC-crRNA region of the integrated
139 Lenti-U6^{BC}-cr*Nf1/Rasa1/Pten*-Cre vectors from bulk tumor-bearing lungs (Tuba-seq^{Ultra})[21,23]. This
140 approach enabled the precise quantification of the number of cancer cells in each clonal tumor, the
141 number of tumors in each mouse, and the relative efficiency of each guide (**Figure 3a**). Overall
142 tumor burden normalized to viral titer was more than 10-fold greater in *H11*$^{LSL\text{-}Cas12a}$ than *KT* mice
143 (**Figure 3b**). We also assessed the number of clonal barcoded tumors in each mouse and found
144 that *H11*$^{LSL\text{-}Cas12a}$ mice had 2-fold more tumors on average than *Kras*$^{LSL\text{-}G12D}$ mice when corrected
145 for viral titer (**Figure 3c**). These results are consistent with the high tumorigenic potential of lung
146 epithelial cells with combined inactivation of *Nf1*, *Rasa1*, and *Pten*[20,24].

147 Tumor sizes in *H11*$^{LSL\text{-}Cas12a}$ mice were dramatically larger than in *KT* mice, with the log-
148 normal mean tumor size around 4-fold greater in *H11*$^{LSL\text{-}Cas12a}$ mice (**Figure 3d**), suggesting
149 increased tumor growth of cr*Nf1/Rasa1/Pten* tumors compared to those driven by oncogenic
150 KRAS. Finally, each of the 9 crRNAs (**Figure 3e-f**) and 27 crRNA arrays (**Supplementary Figure**
151 **2a-b**) generated relatively similar tumor numbers and sizes. These results indicate efficient gene
152 inactivation and multiplexed somatic genome editing in *H11*$^{LSL\text{-}Cas12a}$ mice.
153

154 **Induction of small-cell lung cancer through the Cas12a-mediated inactivation of *Rb1, Trp53*,**
155 **and *Rbl2***

156 Small-cell lung cancer (SCLC) is a neuroendocrine cancer that has been modeled in mice
157 through Cre/lox-mediated, and more recently Cas9-mediated, inactivation of *Rb1*, *Trp53* and
158 *Rbl2*[25,26]. We generated a lentiviral vector expressing Cre and a pre-crRNA array with all
159 combinations of three guides targeting *Rb1*, *Trp53*, and *Rbl2* to create 27 vectors for combinatorial
160 gene inactivation (Lenti-U6^{BC}-cr*Rb1/Trp53/Rbl2*-Cre; **Figure 4a**). We transduced *H11*$^{LSL\text{-}Cas12a}$
161 mice (some of which also contained an *R26*$^{LSL\text{-}Tomato}$ allele) and wild-type negative control mice
162 with Lenti-U6^{BC}-cr*Rb1/Trp53/Rbl2*-Cre (**Figure 4b**). After 18 weeks, transduced *H11*$^{LSL\text{-}Cas12a}$
163 mice had high lung tumor burden (**Figure 4c-d**). Tumors in these mice included UCHL1^{positive}
164 bronchiolar early-stage SCLC, along with more poorly differentiated regions (**Figure 4e**). Cancer
165 cells stained positive for the Cas12a HA tag (**Figure 4e**). Amplification of the BC-crRNA region
166 from bulk tumor-bearing lungs, high-throughput sequencing, and Tuba-seq^{Ultra} analysis revealed
167 that *H11*$^{LSL\text{-}Cas12a}$ mice transduced with Lenti-U6^{BC}-cr*Rb1/Trp53/Rbl2*-Cre had large numbers of
168 clonal tumors and high tumor burden, consistent with robust tumor growth (**Figure 4f-g**).
169 Microdissected tumors had indels at the targeted genomic sites (**Figure 4h**). Quantitative analysis

170 of the crRNA arrays in tumors showed that different crRNAs generated similar tumor numbers
171 and sizes (**Figure 4i-j**). Thus, *H11*$^{LSL\text{-}Cas12a}$ mice enabled rapid and efficient generation of this
172 recalcitrant cancer type.
173
174 **Generation of autochthonous PDAC with inactivation of *Trp53*, *Cdkn2a*, and *Smad4***
175 *TP53*, *CDKN2A*, and *SMAD4* are the three most frequently mutated tumor suppressor
176 genes in human pancreatic ductal adenocarcinoma (PDAC), and many diagrams of the genomic
177 progression of this cancer type show the acquisition of mutations/alterations in all three of these
178 genes[27,28]. However, despite extensive work to investigate these tumor suppressor genes in
179 pancreatic carcinogenesis *in vivo*[29–35], a model in which all three tumor suppressor genes are
180 inactivated has yet to be published. To determine whether Cas12a-mediated somatic genome
181 editing would also be efficient in adult pancreatic epithelial cells, we generated a lentiviral vector
182 expressing Cre and pre-crRNA arrays with three gRNAs targeting *Trp53*, *Cdkn2a*, and *Smad4*
183 (Lenti-U6^{BC}-cr*Trp53/Cdkn2a/Smad4*-Cre; **Figure 5a**).
184 We delivered this pool to the pancreata of *KT;H11*$^{LSL\text{-}Cas12a}$, Cas12a-negative *KT*, and
185 *H11*$^{LSL\text{-}Cas12a}$ mice through retrograde pancreatic ductal injection (**Figure 5b**)[36]. Several
186 *KT;H11*$^{LSL\text{-}Cas12a}$ mice developed large multifocal pancreatic tumors as early as 6 weeks after
187 transduction, with some also showing metastatic dissemination to the liver (**Figure 5c-e**). While
188 *KT* mice only developed PanIN lesions, *KT;H11*$^{LSL\text{-}Cas12a}$ mice developed large, Cas12a-expressing
189 primary tumors, including poorly-differentiated PDAC with cytological atypia and smaller
190 Cytokeratin-19^{positive} mucinous regions with desmoplastic stroma and lobular structures (**Figure 5f**
191 and **Supplementary Figure 3a-b**). The pancreata of transduced *H11*$^{LSL\text{-}Cas12a}$ mice appeared

192 entirely normal, suggesting that even the combined inactivation of these three tumor suppressors
193 has minimal effect in the absence of oncogenic KRAS (**Figure 4f**).

194 Tuba-seq^{Ultra} analysis indicated that *KT;H11$^{LSL\text{-}Cas12a}$* and *KT* mice developed similar
195 numbers of clonal expansions/tumors, consistent with the importance of oncogenic KRAS in
196 tumorigenesis (**Figure 5g**). However, *KT;H11$^{LSL\text{-}Cas12a}$* mice had much larger tumors and thus
197 higher tumor burden (**Figure 5h** and **Supplementary Figure 3c-d**). Analysis of bulk tissue
198 uncovered indels at all target sites (**Supplementary Figure 3e**). Tumors with each of the 9 crRNAs
199 had similar tumor number and size, further underscoring the broad efficiency of Cas12a-mediated
200 gene inactivation (**Figure 5i** and **Supplementary Figure 3f**).

201 Lentiviral vectors generated as a pool suffer from lentiviral template switching during
202 reverse transcription, which can shuffle different elements[37]. We observed minimal
203 recombination-mediated shuffling of guides between different crRNA arrays (**Supplementary**
204 **Figure 4a-f**), likely due to the short distance between guides in Cas12a-based crRNA arrays, in
205 contrast to Cas9-based approaches[37,38]. These data highlight the versatility of somatic Cas12a-
206 mediated gene inactivation to generate novel and clinically relevant complex cancer genotypes.

207

208 **DISCUSSION**

209 In this study, we used Cas12a mice and 3-guide crRNA arrays to rapidly generate complex
210 genotypes in somatic cells. By synthesizing and cloning arrays in a simple pooled manner, this
211 approach should enable the rapid generation of numerous complex genotypes in parallel,
212 dramatically increasing both the scale and the rate at which new disease models with complex
213 genotypes can be studied. Previous *in vitro* studies have employed as many as 25 guides together[7],
214 suggesting that many loci could be targeted together *in vivo* with this transgenic model.

215 We applied somatic CRISPR/Cas12a genome editing initially to study cancer, as cancer
216 has tremendous genomic complexity, yet the genetically engineered mouse models that have been
217 used to study these diseases generally have only a few designed genetic changes. While this has
218 enabled a reductionist approach to uncover key phenotypes controlled by different genes in cancer,
219 it has also limited our ability to model and understand key aspects of cancer that are driven by
220 combinations of genomic alterations. For instance, engineered mouse models often fail to develop
221 spontaneous metastases and those that do rarely metastasize to all organs commonly observed in
222 humans[2]. Indeed, metastases tend to have a greater degree of genomic complexity than primary
223 tumors[39], so modeling metastatic cancer in mice may be facilitated by the generation of tumors
224 with additional engineered alterations.

225 While Cre/lox- and CRISPR/Cas9-mediated somatic genome editing have been used to
226 generate cancer models driven by complex combinations of loss of function alleles, the generation
227 of new models remains time-consuming[2]. Furthermore, given the complexity of genotypes within
228 human tumors, the generation of a single model of a given cancer type (*e.g.* our model of oncogene-
229 negative lung adenocarcinoma)[20] should not be seen as a model for all patients with that broad
230 class of tumors. Here, we have developed enAsCas12a mice to close the gap between the
231 complexity of human tumors and the relative simplicity of genetically engineered mouse models.

232 While our study focused on the use of Cas12a for multiple gene inactivation in cancer
233 models, this system is versatile and should have numerous applications within and beyond cancer
234 modeling. Cas12a-generated staggered DNA breaks could make it more suitable for the
235 introduction of exogenous DNA sequences through homology-directed repair[9]. Furthermore,
236 while we used delivery of lentiviral Cre driven by a ubiquitous promoter to initiate Cas12a
237 expression and editing, use of Cre driven by more specific promoters would enable control of

238 Cas12a expression in particular cell types of interest. Somatic Cas12a-mediated genome editing
239 may also be well-suited for generating chromosomal rearrangements, such as oncogenic
240 translocations that require the simultaneous targeting of pairs of loci, as well as the generation of
241 panels of larger deletions. The multiplicity of Cas12a targeting could make it suitable for modeling
242 even more complex mutational states, such as chromothripsis or aneuploidy (through
243 chromosomal destruction). Finally, transgenic Cas12a in our models obviates the need for
244 exogenous delivery of the large (4 kb) Cas12a gene and negates concerns of pre-existing immunity,
245 which has been shown to dramatically affect cells with exogenous Cas9 expression[40].

246 Compared to Cas9, Cas12a creates more diverse indels and continues cutting its target loci
247 for longer due to the greater distance between its PAM and cleavage sites[41]. As a result, we
248 previously used Cas12a to generate an evolving barcode system to map cellular phylogenies[41].
249 Incorporation of this system into *in vivo* models of development and disease could complement
250 Cas9-based approaches, and the multiplexed ability of Cas12a crRNA expression could allow
251 lineage tracing in combination with gene inactivation. This could dramatically increase our ability
252 to both generate and study complex genotypes[42–45].

253 The generation of somatic cells with complex genotypes could be of broad value, both in
254 cancer modeling and beyond. Somatic genome editing with Cas9 transgenic mice has enabled
255 rapid analysis of the *in vivo* effects of genetic alterations in neuroscience[46–49], cancer[22,50–53],
256 immunology[54], and other fields[55,56]. These Cas12a transgenic mice will enable the generation of
257 pairwise and higher-order combinations of genetic alterations to be generated in cell types of
258 interest to map complex phenotypes to complex genotypes and improve our understanding of
259 human disease.

260

261 **FIGURE LEGENDS**

262

263 **Figure 1. Generation of Cre-regulated and constitutive Cas12a mice**

264 **a.** Schematic of the *H11*$^{LSL\text{-}Cas12a}$ transgene. Enhanced AsCas12a containing several substitutions
265 to increase on-target efficiency and PAM binding sequence range (Kleinstiver *et al.* (2019). *Nature*
266 *Biotechnology*), has two nuclear localization sequences (NLS), and three HA tags at the C-
267 terminus (Liu *et al.* (2019), *Nucleic Acids Research*), controlled by Cre-mediated removal of the
268 LoxP-Stop-LoxP (LSL) cassette.

269 **b.** PCR genotyping of mice of the indicated *H11*$^{LSL\text{-}Cas12a}$ and wild-type (*WT*) genotypes.

270 **c.** Western blots on tail tip fibroblasts from *H11*$^{LSL\text{-}Cas12a}$ and wild-type control mice 3 days after
271 Adeno-Cre (Cre) treatment. Cas12a was detected by both anti-HA and anti-Cas12a antibodies.
272 αTubulin shows loading.

273 **d.** Schematic of the *H11*^{Cas12a} transgene, following Cre-mediated removal of the LSL cassette.

274 **e.** Western blots on tissue lysates from *H11*$^{Cas12a/WT}$ or *H11*$^{LSL\text{-}Cas12a/WT}$ mice. αTubulin shows
275 loading.

276 **f.** Immunohistochemical staining for the HA tag on Cas12a on liver sections from the indicated
277 genotypes of mice. Scale bars, 25 μm.

278

279 **Figure 2. Rapid and efficient generation of oncogene-negative lung tumors through Cas12a-**
280 **mediated coincident inactivation of three tumor suppressor genes**

281 **a.** Lenti-U6^{BC}-cr*Nf1/Rasa1/Pten*-Cre pool has guides targeting *Nf1*, *Rasa1*, and *Pten*. Each gene
282 is targeted by three crRNAs in all combinations.

283 **b.** Design of a lentiviral vector that expresses Cre recombinase and has a pre-crRNA array with
284 three spacers (guides) downstream of a bovine U6 promoter with an integrated barcode region.
285 **c.** Intratracheal delivery of Lenti-U6^{BC}-cr*Nf1/Rasa1/Pten*-Cre to *H11*$^{LSL\text{-}Cas12a}$, *Kras*$^{LSL\text{-}G12D}$;*R26*$^{LSL\text{-}Tom}$ (*KT*), and wild-type (*WT*) mice. Viral titer (infectious units, ifu) and mouse
287 numbers are indicated.
288 **d.** Lung weights from mice of the indicated genotypes 9 weeks after transduction with Lenti-U6^{BC}-
289 cr*Nf1/Rasa1/Pten*-Cre. Each dot represents a mouse. Means +/- standard deviation are indicated.
290 **e.** Light (upper) and Tomato fluorescent (lower) images of lung lobes from the indicated genotypes
291 of mice 9 weeks after transduction with Lenti-U6^{BC}-cr*Nf1/Rasa1/Pten*-Cre. Dashed lines outline
292 tissues. Tumors are Tomato-positive due to recombination of the *R26*$^{LSL\text{-}Tomato}$ allele. Scale bars, 5
293 mm.
294 **f.** Hematoxylin & eosin (upper), NKX2-1 (middle), and UCHL1 (lower) staining of lung sections
295 from the indicated genotypes. Scale bars, 100 μm.
296 **g.** Immunohistochemical staining for the Cas12a HA tag on lung tissue from representative *H11*$^{LSL\text{-}Cas12a}$
297 and *WT* mice transduced with Lenti-U6^{BC}-cr*Nf1/Rasa1/Pten*-Cre. Scale bars, 100 μm.
298 **h.** Indel frequencies for genomic regions targeted by each crRNA within bulk tumor-bearing lung
299 tissue from *H11*$^{LSL\text{-}Cas12a}$ mice. Means +/- standard deviation of three tumor-bearing lungs are
300 shown.
301
302 **Figure 3. Integration of crRNA arrays with tumor barcoding enables quantification of tumor**
303 **initiation and tumor size**
304 **a.** Schematic of tumor barcoding with high-throughput BC-crRNA sequencing to determine the
305 size of each Cas12a-induced clonal tumor.

306 **b.** Total number of neoplastic cells (Total tumor burden) in each mouse normalized to viral titer.
307 Each dot represents a mouse, and the bars are means. P-value calculated with Wilcoxon rank-sum
308 test.
309 **c.** Number of tumors in each mouse normalized to viral titer. Each dot represents a mouse, and the
310 bars are means. P-value calculated with Wilcoxon rank-sum test.
311 **d.** Mean tumor size given a log-normal tumor size distribution. Each dot represents a mouse, and
312 bars are means. P-value calculated with Wilcoxon rank-sum test.
313 **e.** Number of tumors for each crRNA (guide) relative to the median value for each gene. 95%
314 confidence intervals are shown.
315 **f.** Mean tumor size assuming a log-normal distribution for each crRNA (guide) relative to the
316 median value for each gene. 95% confidence intervals are shown.
317
318 **Figure 4. Induction of small-cell lung cancer through the simultaneous Cas12a-mediated**
319 **inactivation of *Trp53*, *Rb1* and *Rbl2***
320 **a.** Lenti-U6^{BC}-cr*Trp53/Rb1/Rbl2*-Cre pool has guides targeting *Trp53*, *Rb1*, and *Rbl2*. Each gene
321 is targeted by three crRNAs in all 27 combinations.
322 **b.** Intratracheal delivery of Lenti-U6^{BC}-cr*Trp53/Rb1/Rbl2*-Cre to *H11*$^{LSL\text{-}Cas12a}$ and wild-type (*WT*)
323 mice. Viral titer (infectious units, ifu) and mouse numbers are indicated.
324 **c.** Lung weights from mice of the indicated genotypes 18 weeks after transduction with Lenti-
325 U6^{BC}-cr*Trp53/Rb1/Rbl2*-Cre. Each dot represents a mouse. Mean +/- standard deviation is
326 indicated.
327 **d.** Light (upper) and Tomato fluorescent (lower) images of lung lobes from the indicated genotypes
328 of mice 18 weeks after transduction with Lenti-U6^{BC}-cr*Trp53/Rb1/Rbl2*-Cre. Dashed line outlines

329 tissue. Tumors are Tomato-positive due to recombination of the *R26*$^{LSL\text{-}Tomato}$ allele. Scale bars, 5
330 mm.
331 **e.** Hematoxylin & eosin (upper), UCHL1 (middle) and HA tag (lower) staining of lung sections
332 from an *H11*$^{LSL\text{-}Cas12a}$ mouse. Scale bars, 100 μm.
333 **f.** Total number of neoplastic cells (Total tumor burden) in each mouse normalized to viral titer.
334 Each dot represents a mouse, and the bar is the mean.
335 **g.** The number of tumors in each mouse normalized to viral titer. Each dot represents a mouse, and
336 the bar is the mean.
337 **h.** Indel frequencies for genomic regions targeted by each crRNA within micro-dissected tumor
338 tissue from *H11*$^{LSL\text{-}Cas12a}$ mice. Symbol shapes and colors identify values from the same sample.
339 Bars represent means.
340 **i,j.** Number of tumors (**i**) and mean tumor size assuming a log-normal distribution (**j**) for each
341 crRNA (guide) relative to the median value for each gene. 95% confidence intervals are shown.
342
343 **Figure 5. Rapid generation of PDAC through somatic Cas12a-mediated inactivation of**
344 **commonly mutated tumor suppressor genes**
345 **a.** Lenti-U6^{BC}-cr*Trp53/Cdkn2a/Smad4*-Cre pool has guides targeting *Trp53*, *Cdkn2a*, and *Smad4*.
346 Each gene is targeted by three crRNAs in all 27 combinations.
347 **b.** Intrapancreatic delivery of Lenti-U6^{BC}-cr*Trp53/Cdkn2a/Smad4*-Cre to *Kras*$^{LSL\text{-}G12D}$*;R26*$^{LSL\text{-}Tom}$
348 (*KT*), *KT;H11*$^{LSL\text{-}Cas12a}$, and *H11*$^{LSL\text{-}Cas12a}$ mice. Viral titer (infectious units, ifu) and mouse numbers
349 are indicated.
350 **c.** Survival curve of mice of the indicated genotypes transduced with Lenti-U6^{BC}-
351 cr*Trp53/Cdkn2a/Smad4*-Cre.

352 **d.** Light (upper) and fluorescent Tomato (lower) pancreas images from the indicated genotypes of
353 mice 6 weeks (*KT;H11*$^{LSL\text{-}Cas12a}$) or 11 weeks (*KT*) after transduction with Lenti-U6^{BC}-
354 cr*Trp53/Cdkn2a/Smad4*-Cre. Dashed lines outline tissues. Scale bars, 5 mm.
355 **e.** Light and fluorescent Tomato images of a liver lobe from a *KT;H11*$^{LSL\text{-}Cas12a}$ mouse. Dashed
356 line outlines tissue. Scale bars, 5 mm.
357 **f.** Immunohistochemistry images of pancreas sections from the indicated genotypes, showing
358 hematoxylin & eosin (H&E; upper) and Alcian Blue (AB; lower) staining. *KT;H11*$^{LSL\text{-}Cas12a}$ panels
359 show representative regions with poorly differentiated sarcomatoid carcinoma (left; approximately
360 80-90% of tumor area) and more differentiated areas with mucinous cells and some lobular
361 structure (right). Scale bars, 100 μm.
362 **g.** The number of tumors in each mouse normalized to viral titer. Each dot represents a mouse, and
363 bars are means. Note that two *H11*$^{LSL\text{-}Cas12a}$ mice did not have detectable tumor burden and are not
364 plotted. P-value calculated with Wilcoxon rank-sum test.
365 **h.** Mean tumor size given a log-normal tumor size distribution. Each dot represents a mouse, and
366 bars are means. Note that two *H11*$^{LSL\text{-}Cas12a}$ mice did not have detectable tumor burden and are not
367 plotted. P-value calculated with Wilcoxon rank-sum test.
368 **i.** Number of tumors for each crRNA (guide) relative to the median value for each gene. 95%
369 confidence intervals are shown.
370
371
372
373
374

375 **METHODS**

376

377 **Generation of the *H11*$^{LSL\text{-}Cas12a}$ transgenic allele**

378 A targeting vector containing 5' and 3' homology arms flanking the chicken beta-actin
379 /CMV enhancer/gamma globulin splice acceptor (CAGGS) promoter, *loxP*-STOP(6xSV40
380 polyA)-*loxP* cassette (LSL), enhanced *Acidaminococcus sp.* Cas12a
381 (E174R/N282A/S542R/K548R; enAsCas12a)[13], a nucleoplasmin nuclear localization signal
382 (NLS), a 3xHA epitope sequence, an SV40 NLS[19], and a rabbit β-globin polyadenylation signal
383 (RBG pA) was used to generate the *H11*$^{LSL\text{-}Cas12a}$ knock-in mice. An sgRNA targeting the mouse
384 *Hipp11* (*H11*) locus (GAACACTAGTGCACTTATCCTGG), the targeting vector, and Cas9
385 mRNA were co-injected into fertilized C57BL/6J mouse oocytes (Cyagen Biosciences). F0
386 founder animals were identified by PCR followed by sequence analysis. A founder mouse was
387 bred with C57BL/6J mice to establish the *H11*$^{LSL\text{-}Cas12a}$ line. *H11*$^{LSL\text{-}Cas12a}$ mice were crossed to
388 CMV-Cre "deleter" mice to generate the constitutive *H11*^{Cas12a} mice. PCR genotyping for the
389 *H11*$^{LSL\text{-}Cas12a}$ transgene was performed with the following primers: forward, 5'
390 ATGCCATCATGCTCTCACTGC 3'; reverse, 5' GGCTATGAACTAATGACCCCGTAATTG
391 3'; alternative reverse, 5' CTTGTGGGTCTTCCACCTTTCTT 3'. PCR genotyping to distinguish
392 *H11*$^{LSL\text{-}Cas12a}$ from *H11*^{Cas12a} was performed with the following primers: forward, 3'
393 AGGTCGAGGGACCTAATAACTTCG 5'; alternative forward, 5'
394 ATCTGTGCGGAGCCGAAATC 3'; reverse, 5' TGCGTGCTTTGTCTTCCTCG 3'.

395

396

397

398 **Design, generation, barcoding, and production of lentiviral vectors**

399 Pre-crRNA arrays with three guides were designed with diverse direct repeat sequences
400 flanking each guide[11], with BsmBI cut sites on both ends of the array (all guide and array
401 sequences in **Supplementary Table 1**). Guides for enAsCas12a were designed using CRISPick
402 for the Mouse GRCm38 reference genome (NCBI RefSeq v.108.20200622)[11,57]. Arrays were
403 ordered as single-stranded DNA pools (Twist Biosciences) containing all 27 combinations of 3
404 guides for each of the 3 genes targeted in an array. Barcoded lentiviral vector backbones were
405 created by cloning a 98 bp oligo with a 16-nucleotide diverse barcode (BC) and two BsmBI
406 restriction sites into the 3' end of the bovine U6 promoter with Gibson Assembly (NEBuilder HiFi,
407 New England Biosciences) in a vector also containing PGK-Cre recombinase[23]. After low-cycle
408 PCR amplification, pre-crRNA arrays were ligated via Golden Gate Assembly with BsmBI into
409 the barcoded vector backbone. The cloning product was then electroporated into competent *E. coli*
410 (C3020K, New England Biosciences) and plated onto LB-ampicillin plates. To ensure sufficient
411 barcode diversity for Tuba-seq^{Ultra} sequencing and delineation of tumors, ~10^6 colonies were
412 collected for each Lenti-U6^{BC}-crRNA-Cre pool.

413 Lentiviral vectors were produced using polyethylenimine (PEI)-based transfection of 293T
414 cells with delta8.2 and VSV-G packaging plasmids in 15 cm cell culture plates. Sodium butyrate
415 (B5887, Sigma Aldrich) was added 8 hours after transfection to achieve a final concentration of
416 20 mM. Media was refreshed 24 hours after transfection. 20 mL of virus-containing supernatant
417 was collected 36, 48, and 60 hours after transfection. The three collections were then pooled and
418 concentrated by ultracentrifugation (112,000 g for 1.5 hours), resuspended overnight in 120 μL
419 PBS, and then frozen at -80°C. Viruses were titered against a lab standard of known titer.

420

421 **Mice and tumor initiation**

422 The use of mice for this study was approved by the Institutional Animal Care and Use
423 Committee at Stanford University, protocol number 26696. CMV-Cre
424 (RRID:IMSR_JAX:006054)[58], *Kras*$^{LSL\text{-}G12D/+}$ (RRID:IMSR_JAX:008179)[59] and *R26*$^{LSL\text{-}tdTomato}$
425 (RRID:IMSR_JAX:007914)[60] mice were on a C57BL/6J background. *H11*$^{LSL\text{-}Cas12a}$ mice
426 (JAX:038388) and *H11*^{Cas12a} mice (JAX:038389) are available through the Jackson Laboratory.

427 Lung tumors were initiated by intratracheal delivery of 60 µL of lentiviral vectors in PBS
428 to isoflurane-anesthetized mice. Pancreatic tumors were initiated by retrograde ductal delivery of
429 150 µL of lentiviral vectors in PBS to isoflurane-anesthetized mice as previous described, and
430 mice were injected intraperitoneally with 100 µg/kg cerulein (C9026, Sigma-Aldrich) every hour
431 for 8 hours over two consecutive days, two weeks after lentiviral delivery[36]. For small-cell lung
432 cancer tumors, mice were pre-treated with naphthalene[53]. Briefly, corn oil (C8267, Sigma-Aldrich)
433 was filter-sterilized with a 0.22 µm filter and aliquoted into 5 mL portions. Naphthalene was then
434 dissolved into the corn oil vehicle at a concentration of 50 mg/mL before it was administered into
435 mice via intraperitoneal injections at a dosage of 200 mg/kg. Roughly 46-48 hours later, mice were
436 administered virus intratracheally and supplemented with a bowl of DietGel76A (72-07-5022,
437 ClearH2O) food to promote recovery. Infectious units (ifu) of lentivirus used for each experiment
438 are indicated in each respective figure.

439

440 **Histology and immunohistochemistry**

441 Tissues were fixed in 4% formalin for 24 hours, stored in 70% ethanol, and paraffin-
442 embedded. 4 µm thick sections were used for Hematoxylin and Eosin staining and
443 immunohistochemistry. Immunohistochemistry was performed using an Avidin/Biotin Blocking

444 Kit (SP-2001, Vector Laboratories), Avidin-Biotin Complex kit (PK-4001, Vector Laboratories),
445 and DAB Peroxidase Substrate Kit (SK-4100, Vector Laboratories) following standard protocols.
446 Alcian Blue and Trichrome stains were performed following standard protocols (Histo-Tec
447 Laboratory, Inc.). The following primary antibodies were used: anti-HA (3724, Cell Signaling
448 Technology), anti-TTF1 (NKX2-1; ab76013, Abcam), anti-CK19 (Ab2133570, TROMA-III,
449 Developmental Study Hybridoma Bank), and anti-UCHL1 (HPA005993, Sigma-Aldrich).
450
451 **Western blot analyses**
452 For immunoblotting, cells and homogenized tissues were lysed in Cell Lysis Buffer (Cell
453 Signaling Technology) containing a complete mini-protease inhibitor cocktail (Roche), then equal
454 quantities of protein lysate (3-10 μg) were separated by SDS-PAGE using 4–12% gradient gels
455 (Invitrogen) and transferred to PVDF membranes. Membranes were blocked with 5% milk in PBS
456 with 0.1% Tween 20 (PBST) for 1 hour at room temperature, followed by incubation with primary
457 antibodies diluted in PBST with 5% milk overnight at 4ºC. After 4x15 minute washes with PBST,
458 membranes were incubated with an HRP-conjugated goat anti-rabbit secondary antibody (12-348,
459 Sigma-Aldrich) diluted 1:5000 in PBST with 5% milk. After 4x15 minute washes with PBST,
460 protein expression was then visualized with enhanced chemiluminescence reagents (PI80196,
461 Fisher Scientific). Primary antibodies were used at the following dilutions: rabbit anti-HA, 1:1000
462 (3724, Cell Signaling); rabbit anti-Cas12a, 1:1000 (19984, Cell Signaling); and rabbit anti-alpha-
463 Tubulin, 1:2000 (2144, Cell Signaling).
464
465
466

467 **Analysis of indels at target sites**

468 The target sites for each crRNA were PCR-amplified from genomic DNA extracted from
469 bulk tumor-bearing tissue (**Figure 2h** and **Supplementary Figure 3e**) or microdissected tumors
470 (**Figure 4h**) using GoTaq Green® Mastermix (Promega) and the primer pairs listed in
471 **Supplementary Table 2**. Microdissected tumors were isolated under a dissecting microscope;
472 however, due to the high tumor burden, samples may have contained more than one tumor.

473 Amplicons were run on 1% agarose gels, gel-extracted (QIAquick PCR & Gel Cleanup Kit,
474 Qiagen), and Sanger sequenced (Elim Biopharm, Inc). The Sanger sequencing traces were
475 analyzed with TIDE[61] to estimate the percent of the DNA with indels at each site. As these lungs
476 each contain many clonal tumors, the DNA should be a mix of that from non-neoplastic cells
477 (normal lung and stromal cells), tumors with indels at that site, and tumor with indels at the target
478 sites of the other crRNAs targeting that gene.

479

480 **Tuba-seq^{Ultra} library preparation and analysis**

481 Benchmark control cell lines containing unique barcodes (50,000 cells each) were added
482 to each lung sample prior to lysis to enable the calculation of the absolute number of neoplastic
483 cells in each tumor[23]. Bulk tumor-bearing tissues were homogenized in 6 mL of cell lysis buffer
484 (Puregene, 158063, Qiagen) using a FastPrep-24 5G tissue homogenizer (116005500, MP
485 Biomedicals) and digested overnight with proteinase K (AM2544, Life Technologies). To remove
486 RNA, samples were incubated with RNase A prior to genomic DNA extraction using a Puregene
487 kit according to the manufacturer's recommended protocol. Q5 High-Fidelity 2x Master Mix
488 (M0494X, New England Biolabs) was used to amplify the U6-BC-crRNA region from 32 µg of
489 genomic DNA in a total reaction volume of 800 µL per sample using unique dual-indexed primers

490 as described[23]. The concentration of the amplified barcode product in each PCR was measured
491 using D1000 screentape reagents (5067-5582, Agilent Technologies) and the Tapestation
492 instrument (Agilent Technologies). Amplicons were pooled at equal molar ratios of barcode
493 product, normalized to the estimated burden of tumors in each mouse lung sample (measured lung
494 mass minus an estimated normal lung weight of 0.15 g). Pooled PCR products were purified using
495 Agencourt AMPure XP beads (A63881, Beckman Coulter) using a double size selection protocol
496 and sequenced on the Illumina NextSeq 6000 platform (read length 2x150bp) for barcode analysis
497 and MiSeq (2x300) for crRNA array analysis.

498 Paired-end reads were processed with regular expressions to identify the three gRNA
499 sequences (henceforth referred to as the tumor-genotype) and clonal barcodes. When identifying
500 gRNA sequences, we strictly required a perfect match with the designed sequences. The 12-
501 nucleotide random clonal barcode sequence possesses a high theoretical diversity of approximately
502 4^{12} (> 10^7). Given the virus titer we used ($2x10^5$ or $1x10^6$ infectious units per mouse), there are
503 typically fewer than 10,000 clonal tumors for each tumor-genotype per mouse. As such, the
504 probability of two clonal tumors with the same tumor-genotype possessing two barcodes within a
505 1-hamming distance of each other is extremely low. Consequently, when we encountered low-
506 frequency clonal barcodes within a 1-hamming distance of high-frequency clonal barcodes, we
507 attributed them to sequencing or PCR errors. These low-frequency barcodes were merged with
508 barcodes of higher frequencies. After extracting barcode and crRNA information, we converted
509 the read counts associated with clonal tumors into absolute neoplastic cell numbers. This
510 conversion was accomplished by normalizing the reads of the clonal tumor to the number of reads
511 of the "spike-in" benchmark cell lines added to each sample prior to lung lysis and DNA extraction.
512 We imposed a minimum tumor size cutoff of 300 cells for downstream analysis.

513

514 **Characterization of overall tumor growth and initiation**

515 To quantify tumor growth, we used the log-normal mean (LN mean) tumor size, which is
516 the maximum-likelihood estimate of mean tumor size, assuming a log-normal tumor size
517 distribution. In addition to the tumor size metric, we characterized the effects of gene inactivation
518 on tumorigenesis by accounting for both the number of tumors ("tumor number") and the
519 cumulative number of neoplastic cells ("tumor burden"). When comparing tumor growth and
520 initiation across different genotypes of mice tumor number and tumor burden are normalized by
521 the amount of virus delivered.

522

523 **Estimation of tumor growth and initiation effects of individual crRNA arrays**

524 To estimate the relative effect of individual crRNAs on tumor growth, we calculated the
525 relative LN mean tumor size by normalizing the LN mean of tumors with a specific crRNA to the
526 average LN mean size of the three crRNAs targeting the same gene. This normalization process
527 extended to the analysis of tumors with specific crRNA arrays, where the relative LN mean tumor
528 size for a tumor with an array was normalized to the mean of all 27 distinct crRNA arrays. Unlike
529 the LN mean tumor size, tumor number is linearly affected by lentiviral titer and is thus sensitive
530 to underlying differences in the representation of each Lenti-U6^{BC}-crRNA-Cre vector in the viral
531 pool. Relative tumor number was computed by initially standardizing the tumor number in Cas12a-
532 expressive mice against that in control mice lacking Cas12a. Subsequently, this standardized tumor
533 number was then normalized using the same methodology applied to the relative LN mean.

534

535

536 **Tumor exclusion based on PCR template shuffling and unexpected crRNA arrays**

537 Ideally, each clonal barcode would be uniquely paired with one crRNA array. However,
538 instances where the same clonal barcode is associated with multiple crRNA arrays have been
539 observed, which may be attributed to several factors: (1) multiple copies of the same barcode
540 molecule ligated to distinct arrays during vector cloning; (2) template switching during lentiviral
541 reverse transcription; and (3) PCR uncoupling throughout library preparation[37,38]. The first two
542 scenarios would yield tumors that accurately reflect the genotype information conveyed by the
543 crRNA array, while the latter scenario would generate spurious tumors (i.e. BC-crRNA reads
544 that do not originate from a genuine tumor in the sample). Such spurious tumors, resulting from
545 PCR uncoupling (a relatively rare event) will typically be markedly smaller than their genuine
546 counterparts. To discern spurious tumors from genuine tumors with the same clonal barcode, we
547 created a reference null distribution of size ratios between large and small tumors by randomly
548 sampling pairs of tumors within the same mouse. When a clonal barcode was found associated
549 with multiple crRNA arrays, we designated the crRNA array with the largest tumor as genuine
550 and others as potentially aberrant. By calculating the size ratio of the genuine to the potential
551 spurious tumor and comparing it against the upper 95th percentile of the reference distribution,
552 we can identify and eliminate most, if not all, spurious tumors.

553 In cases when tumors were found to be associated with crRNA arrays that were not from
554 the "correct" lentiviral libraries, these tumors could have arisen from the coincident transduction
555 of a cell with the "correct" virus and a "contaminating" virus. To eliminate these tumors from the
556 analysis in the most conservative manner, we identified each clonal barcode linked to the
557 "contaminating" vector, a corresponding clonal barcode associated with the "correct" vector that

558 exhibited the most similar tumor size within the same mouse, and excluded both clonal barcodes
559 from further analysis.
560
561 **Cell line generation**
562 Tail tip fibroblasts were generated by mechanically dissociating depilated tail tips,
563 digesting them in 0.25% trypsin (Life Technologies) for 30 minutes, collecting tissue fragments
564 with centrifugation at 500 rcf for 5 minutes, then resuspending and plating in high glucose
565 Dulbecco's Modified Eagle Medium (Life Technologies) containing 20% fetal bovine serum and
566 2% penicillin-streptomycin (Thermo Fisher Scientific).
567
568 **ACKNOWLEDGEMENTS**
569
570 We thank the Stanford Veterinary Animal Care Staff for expert animal care, Greg Charville
571 for advice on histologic characterization of tumors, and members of the Winslow laboratory for
572 helpful comments. J.D.H was supported by an American Cancer Society Fellowship (PF-21-112-
573 01-MM) and a TRDRP Postdoctoral fellowship (T31FT1619). Y.J.T was partly supported by the
574 Canadian Institute of Health Research (CIHR) postdoctoral fellowship (MFE-176568). P.A.R. was
575 supported by the National Science Foundation Graduate Research Fellowship (DGE-2146755) and
576 the Lucille P. Markey Stanford Graduate Fellowship. This work was supported by NIH R01-
577 CA230025 (to M.M.W), NIH P01-CA244114 (to M.M.W.), NIH R01-CA231253 (to M.M.W and
578 D.A.P), NIH R01-CA234349 (to M.M.W and D.A.P.), NIH R35-CA231997 (to J.S.), NIH R35-
579 HG011316 and R01-GM141627 (to L.C.), and in part by the Stanford Cancer Institute support
580 grant (NIH P30-CA124435).

581

582 **References**

583 1. Kersten, K., de Visser, K. E., van Miltenburg, M. H. & Jonkers, J. Genetically engineered
584 mouse models in oncology research and cancer medicine. *EMBO Mol. Med.* **9**, 137–153
585 (2017).
586 2. Hebert, J. D., Neal, J. W. & Winslow, M. M. Dissecting metastasis using preclinical models
587 and methods. *Nat. Rev. Cancer* **23**, 391–407 (2023).
588 3. Murray, C. W. *et al.* An LKB1-SIK Axis Suppresses Lung Tumor Growth and Controls
589 Differentiation. *Cancer Discov.* **9**, 1590–1605 (2019).
590 4. Paul, B. & Montoya, G. CRISPR-Cas12a: Functional overview and applications. *Biomed. J.*
591 **43**, 8–17 (2020).
592 5. Khan, S. & Sallard, E. Current and Prospective Applications of CRISPR-Cas12a in
593 Pluricellular Organisms. *Mol. Biotechnol.* **65**, 196–205 (2023).
594 6. Zetsche, B. *et al.* Multiplex gene editing by CRISPR–Cpf1 using a single crRNA array. *Nat.*
595 *Biotechnol.* **35**, 31–34 (2017).
596 7. Campa, C. C., Weisbach, N. R., Santinha, A. J., Incarnato, D. & Platt, R. J. Multiplexed
597 genome engineering by Cas12a and CRISPR arrays encoded on single transcripts. *Nat.*
598 *Methods* **16**, 887–893 (2019).
599 8. Dede, M., McLaughlin, M., Kim, E. & Hart, T. Multiplex enCas12a screens detect functional
600 buffering among paralogs otherwise masked in monogenic Cas9 knockout screens. *Genome*
601 *Biol.* **21**, 1–19 (2020).
602 9. Dai, X. *et al.* Massively parallel knock-in engineering of human T cells. *Nat. Biotechnol.* **41**,
603 1239–1255 (2023).

604 10. Magnusson, J. P., Rios, A. R., Wu, L. & Qi, L. S. Enhanced Cas12a multi-gene
605 regulation using a CRISPR array separator. *eLife* **10**, e66406 (2021).
606 11. DeWeirdt, P. C. *et al.* Optimization of AsCas12a for combinatorial genetic screens in
607 human cells. *Nat. Biotechnol.* **39**, 94–104 (2021).
608 12. Ma, E. *et al.* Improved genome editing by an engineered CRISPR-Cas12a. *Nucleic Acids*
609 *Res.* **50**, 12689–12701 (2022).
610 13. Kleinstiver, B. P. *et al.* Engineered CRISPR–Cas12a variants with increased activities
611 and improved targeting ranges for gene, epigenetic and base editing. *Nat. Biotechnol.* **37**, 276–
612 282 (2019).
613 14. Gier, R. A. *et al.* High-performance CRISPR-Cas12a genome editing for combinatorial
614 genetic screening. *Nat. Commun.* **11**, 3455 (2020).
615 15. Zhang, L. *et al.* AsCas12a ultra nuclease facilitates the rapid generation of therapeutic
616 cell medicines. *Nat. Commun.* **12**, 3908 (2021).
617 16. Vogelstein, B. *et al.* Cancer Genome Landscapes. *Science* **339**, 1546–1558 (2013).
618 17. Aaltonen, L. A. *et al.* Pan-cancer analysis of whole genomes. *Nature* **578**, 82–93 (2020).
619 18. Cerami, E. *et al.* The cBio cancer genomics portal: an open platform for exploring
620 multidimensional cancer genomics data. *Cancer Discov.* **2**, 401–404 (2012).
621 19. Liu, P. *et al.* Enhanced Cas12a editing in mammalian cells and zebrafish. *Nucleic Acids*
622 *Res.* **47**, 4169–4180 (2019).
623 20. Yousefi, M. *et al.* Combinatorial Inactivation of Tumor Suppressors Efficiently Initiates
624 Lung Adenocarcinoma with Therapeutic Vulnerabilities. *Cancer Res.* **82**, 1589–1602 (2022).
625 21. Rogers, Z. N. *et al.* A quantitative and multiplexed approach to uncover the fitness
626 landscape of tumor suppression in vivo. *Nat. Methods* **14**, 737–742 (2017).

627 22. Cai, H. *et al.* A functional taxonomy of tumor suppression in oncogenic KRAS-driven
628 lung cancer. *Cancer Discov.* (2021) doi:10.1158/2159-8290.CD-20-1325.
629 23. Tang, Y. J. *et al.* A functional map of epigenetic regulators in lung carcinogenesis.
630 *Manuscr. Prep.*
631 24. Yousefi, M. *et al.* Fully accessible fitness landscape of oncogene-negative lung
632 adenocarcinoma. *Proc. Natl. Acad. Sci. U. S. A.* **120**, e2303224120 (2023).
633 25. Schaffer, B. E. *et al.* Loss of p130 Accelerates Tumor Development in a Mouse Model
634 for Human Small-Cell Lung Carcinoma. *Cancer Res.* **70**, 3877–3883 (2010).
635 26. Duplaquet, L. *et al.* KDM6A epigenetically regulates subtype plasticity in small cell lung
636 cancer. *Nat. Cell Biol.* **25**, 1346–1358 (2023).
637 27. Iacobuzio-Donahue, C. A., Velculescu, V. E., Wolfgang, C. L. & Hruban, R. H. Genetic
638 basis of pancreas cancer development and progression: insights from whole-exome and
639 whole-genome sequencing. *Clin. Cancer Res. Off. J. Am. Assoc. Cancer Res.* **18**, 4257–4265
640 (2012).
641 28. Halbrook, C. J., Lyssiotis, C. A., Pasca di Magliano, M. & Maitra, A. Pancreatic cancer:
642 Advances and challenges. *Cell* **186**, 1729–1754 (2023).
643 29. Izeradjene, K. *et al.* Kras(G12D) and Smad4/Dpc4 haploinsufficiency cooperate to
644 induce mucinous cystic neoplasms and invasive adenocarcinoma of the pancreas. *Cancer Cell*
645 **11**, 229–243 (2007).
646 30. Hingorani, S. R. *et al.* Trp53R172H and KrasG12D cooperate to promote chromosomal
647 instability and widely metastatic pancreatic ductal adenocarcinoma in mice. *Cancer Cell* **7**,
648 469–483 (2005).

649 31. Bardeesy, N. *et al.* Smad4 is dispensable for normal pancreas development yet critical in
650 progression and tumor biology of pancreas cancer. *Genes Dev.* **20**, 3130–3146 (2006).
651 32. Aguirre, A. J. *et al.* Activated Kras and Ink4a/Arf deficiency cooperate to produce
652 metastatic pancreatic ductal adenocarcinoma. *Genes Dev.* **17**, 3112–3126 (2003).
653 33. Hingorani, S. R. *et al.* Preinvasive and invasive ductal pancreatic cancer and its early
654 detection in the mouse. *Cancer Cell* **4**, 437–450 (2003).
655 34. Whittle, M. C. *et al.* RUNX3 Controls a Metastatic Switch in Pancreatic Ductal
656 Adenocarcinoma. *Cell* **161**, 1345–1360 (2015).
657 35. Bardeesy, N. *et al.* Both p16(Ink4a) and the p19(Arf)-p53 pathway constrain progression
658 of pancreatic adenocarcinoma in the mouse. *Proc. Natl. Acad. Sci. U. S. A.* **103**, 5947–5952
659 (2006).
660 36. Chiou, S.-H. *et al.* Pancreatic cancer modeling using retrograde viral vector delivery and
661 in vivo CRISPR/Cas9-mediated somatic genome editing. *Genes Dev.* **29**, 1576–1585 (2015).
662 37. Hill, A. J. *et al.* On the design of CRISPR-based single-cell molecular screens. *Nat.*
663 *Methods* **15**, 271–274 (2018).
664 38. Hegde, M., Strand, C., Hanna, R. E. & Doench, J. G. Uncoupling of sgRNAs from their
665 associated barcodes during PCR amplification of combinatorial CRISPR screens. *PloS One*
666 **13**, e0197547 (2018).
667 39. Nguyen, B. *et al.* Genomic characterization of metastatic patterns from prospective
668 clinical sequencing of 25,000 patients. *Cell* **185**, 563-575.e11 (2022).
669 40. Li, A. *et al.* AAV-CRISPR Gene Editing Is Negated by Pre-existing Immunity to Cas9.
670 *Mol. Ther. J. Am. Soc. Gene Ther.* **28**, 1432–1441 (2020).

671 41. Hughes, N. W. *et al.* Machine-learning-optimized Cas12a barcoding enables the recovery
672 of single-cell lineages and transcriptional profiles. *Mol. Cell* **82**, 3103-3118.e8 (2022).
673 42. Yang, D. *et al.* Lineage tracing reveals the phylodynamics, plasticity, and paths of tumor
674 evolution. *Cell* **185**, 1905-1923.e25 (2022).
675 43. Li, L. *et al.* A mouse model with high clonal barcode diversity for joint lineage,
676 transcriptomic, and epigenomic profiling in single cells. *Cell* **186**, 5183-5199.e22 (2023).
677 44. Bowling, S. *et al.* An Engineered CRISPR-Cas9 Mouse Line for Simultaneous Readout
678 of Lineage Histories and Gene Expression Profiles in Single Cells. *Cell* **181**, 1410-1422.e27
679 (2020).
680 45. Chan, M. M. *et al.* Molecular recording of mammalian embryogenesis. *Nature* **570**, 77–
681 82 (2019).
682 46. Santinha, A. J. *et al.* Transcriptional linkage analysis with in vivo AAV-Perturb-seq.
683 *Nature* **622**, 367–375 (2023).
684 47. Jin, X. *et al.* In vivo Perturb-Seq reveals neuronal and glial abnormalities associated with
685 autism risk genes. *Science* **370**, eaaz6063 (2020).
686 48. Zheng, X. *et al.* Massively parallel in vivo Perturb-seq reveals cell type-specific
687 transcriptional networks in cortical development. *BioRxiv Prepr. Serv. Biol.*
688 2023.09.18.558077 (2023) doi:10.1101/2023.09.18.558077.
689 49. Lin, R. *et al.* Directed evolution of adeno-associated virus for efficient gene delivery to
690 microglia. *Nat. Methods* **19**, 976–985 (2022).
691 50. Li, B. E. *et al.* In vivo CRISPR/Cas9 screening identifies Pbrm1 as a regulator of myeloid
692 leukemia development in mice. *Blood Adv.* **7**, 5281–5293 (2023).

693 51. Romero, R. *et al.* Keap1 loss promotes Kras -driven lung cancer and results in
694 dependence on glutaminolysis. *Nat. Med.* **23**, 1362–1368 (2017).
695 52. Ng, S. R. *et al.* CRISPR-mediated modeling and functional validation of candidate tumor
696 suppressor genes in small cell lung cancer. *Proc. Natl. Acad. Sci. U. S. A.* **117**, 513–521
697 (2020).
698 53. Lee, M. C. *et al.* A multiplexed in vivo approach to identify driver genes in small cell
699 lung cancer. *Cell Rep.* **42**, 111990 (2023).
700 54. Belk, J. A. *et al.* Genome-wide CRISPR screens of T cell exhaustion identify chromatin
701 remodeling factors that limit T cell persistence. *Cancer Cell* **40**, 768-786.e7 (2022).
702 55. Song, X. *et al.* Genome Editing with AAV-BR1-CRISPR in Postnatal Mouse Brain
703 Endothelial Cells. *Int. J. Biol. Sci.* **18**, 652–660 (2022).
704 56. Thürkauf, M. *et al.* Fast, multiplexable and efficient somatic gene deletions in adult
705 mouse skeletal muscle fibers using AAV-CRISPR/Cas9. *Nat. Commun.* **14**, 6116 (2023).
706 57. Kim, H. K. *et al.* Deep learning improves prediction of CRISPR-Cpf1 guide RNA
707 activity. *Nat. Biotechnol.* **36**, 239–241 (2018).
708 58. Schwenk, F., Baron, U. & Rajewsky, K. A cre-transgenic mouse strain for the ubiquitous
709 deletion of loxP-flanked gene segments including deletion in germ cells. *Nucleic Acids Res.*
710 **23**, 5080–5081 (1995).
711 59. Jackson, E. L. *et al.* Analysis of lung tumor initiation and progression using conditional
712 expression of oncogenic K-ras. *Genes Dev.* **15**, 3243–3248 (2001).
713 60. Madisen, L. *et al.* A robust and high-throughput Cre reporting and characterization
714 system for the whole mouse brain. *Nat. Neurosci.* **13**, 133–140 (2010).

715 61. Brinkman, E. K., Chen, T., Amendola, M. & van Steensel, B. Easy quantitative
716 assessment of genome editing by sequence trace decomposition. *Nucleic Acids Res.* **42**, e168
717 (2014).
718

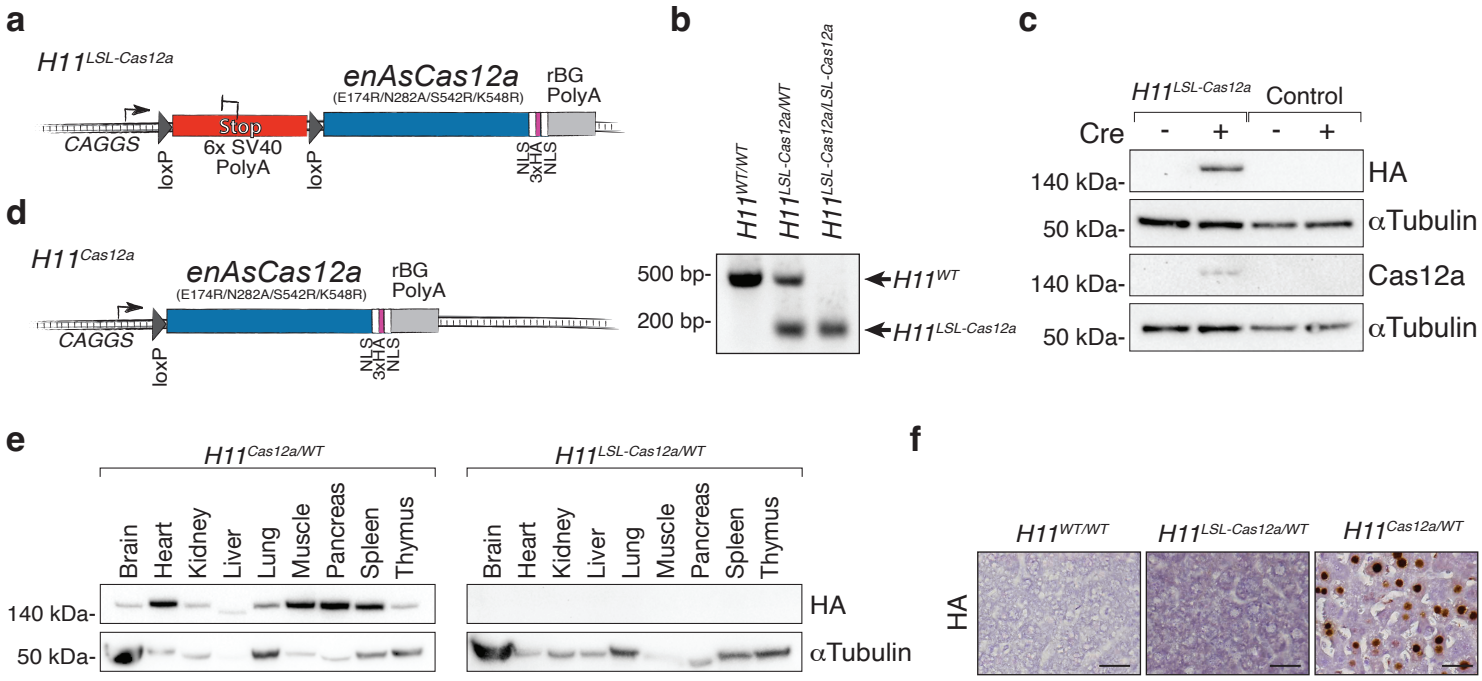

Figure 1. Generation of Cre-regulated and constitutive Cas12a mice

a. Schematic of the *H11*$^{LSL\text{-}Cas12a}$ transgene. Enhanced AsCas12a containing several substitutions to increase on-target efficiency and PAM binding sequence range (Kleinstiver *et al.* (2019). *Nature Biotechnology*), has two nuclear localization sequences (NLS), and three HA tags at the C-terminus (Liu *et al.* (2019), *Nucleic Acids Research*), controlled by Cre-mediated removal of the LoxP-Stop-LoxP (LSL) cassette.

b. PCR genotyping of mice of the indicated *H11*$^{LSL\text{-}Cas12a}$ and wild-type (*WT*) genotypes.

c. Western blots on tail tip fibroblasts from *H11*$^{LSL\text{-}Cas12a}$ and wild-type control mice 3 days after Adeno-Cre (Cre) treatment. Cas12a was detected by both anti-HA and anti-Cas12a antibodies. αTubulin shows loading.

d. Schematic of the *H11*^{Cas12a} transgene, following Cre-mediated removal of the LSL cassette.

e. Western blots on tissue lysates from *H11*$^{Cas12a/WT}$ or *H11*$^{LSL\text{-}Cas12a/WT}$ mice. α–Tubulin shows loading.

f. Immunohistochemical staining for the HA tag on Cas12a on liver sections from the indicated genotypes of mice. Scale bars, 25 µm.

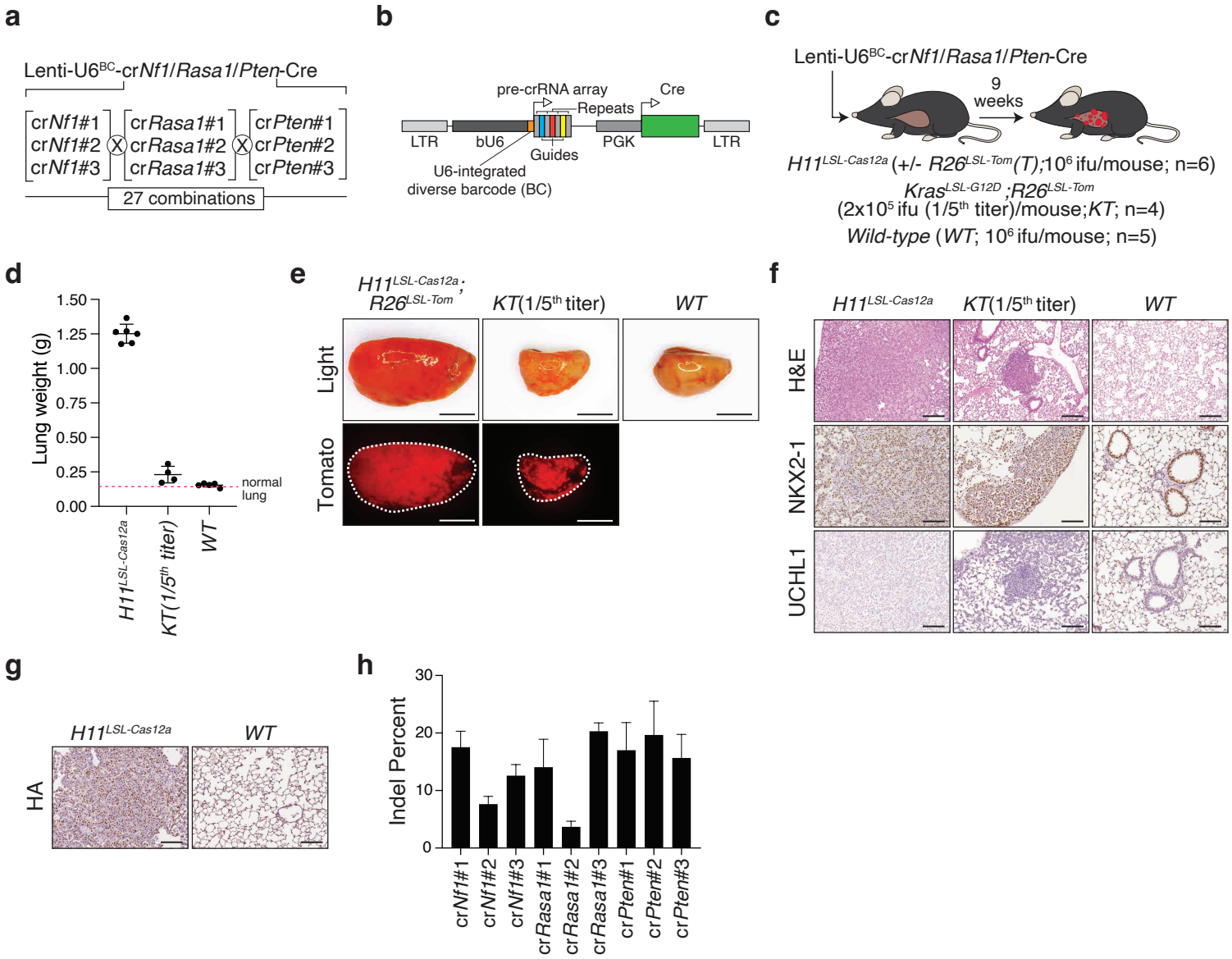

Figure 2. Rapid and efficient generation of oncogene-negative lung tumors through Cas12a-mediated coincident inactivation of three tumor suppressor genes

a. Lenti-U6^{BC}-cr*Nf1/Rasa1/Pten*-Cre pool has guides targeting *Nf1, Rasa1*, and *Pten*. Each gene is targeted by three crRNAs in all combinations.

b. Design of a lentiviral vector that expresses Cre recombinase and has a pre-crRNA array with three spacers (guides) downstream of a bovine U6 promoter with an integrated barcode region.

c. Intratracheal delivery of Lenti-U6^{BC}-cr*Nf1/Rasa1/Pten*-Cre to *H11*$^{LSL\text{-}Cas12a}$, *Kras*$^{LSL\text{-}G12D}$;*R26*$^{LSL\text{-}Tom}$ (*KT*), and *wild-type (WT)* mice. Viral titer (infectious units, ifu) and mouse numbers are indicated.

d. Lung weights from mice of the indicated genotypes 9 weeks after transduction with Lenti-U6^{BC}cr*Nf1/Rasa1/Pten*-Cre. Each dot represents a mouse. Means +/- standard deviation are indicated.

e. Light (upper) and Tomato fluorescent (lower) images of lung lobes from the indicated genotypes of mice 9 weeks after transduction with Lenti-U6^{BC}-cr*Nf1/Rasa1/Pten*-Cre. Dashed lines outline tissues. Tumors are Tomato-positive due to recombination of the *R26*$^{LSL\text{-}Tomato}$ allele. Scale bars, 5 mm.

f. Hematoxylin & eosin (upper), NKX2-1 (middle), and UCHL1 (lower) staining of lung sections from the indicated genotypes. Scale bars, 100 µm.

g. Immunohistochemical staining for the Cas12a HA tag on lung tissue from representative *H11*$^{LSL\text{-}Cas12a}$ and *WT* mice transduced with Lenti-U6^{BC}-cr*Nf1/Rasa1/Pten*-Cre. Scale bars, 100 µm.

h. Indel frequencies for genomic regions targeted by each crRNA within bulk tumor-bearing lung tissue from *H11*$^{LSL\text{-}Cas12a}$ mice. Means +/- standard deviation of three tumor-bearing lungs are shown.

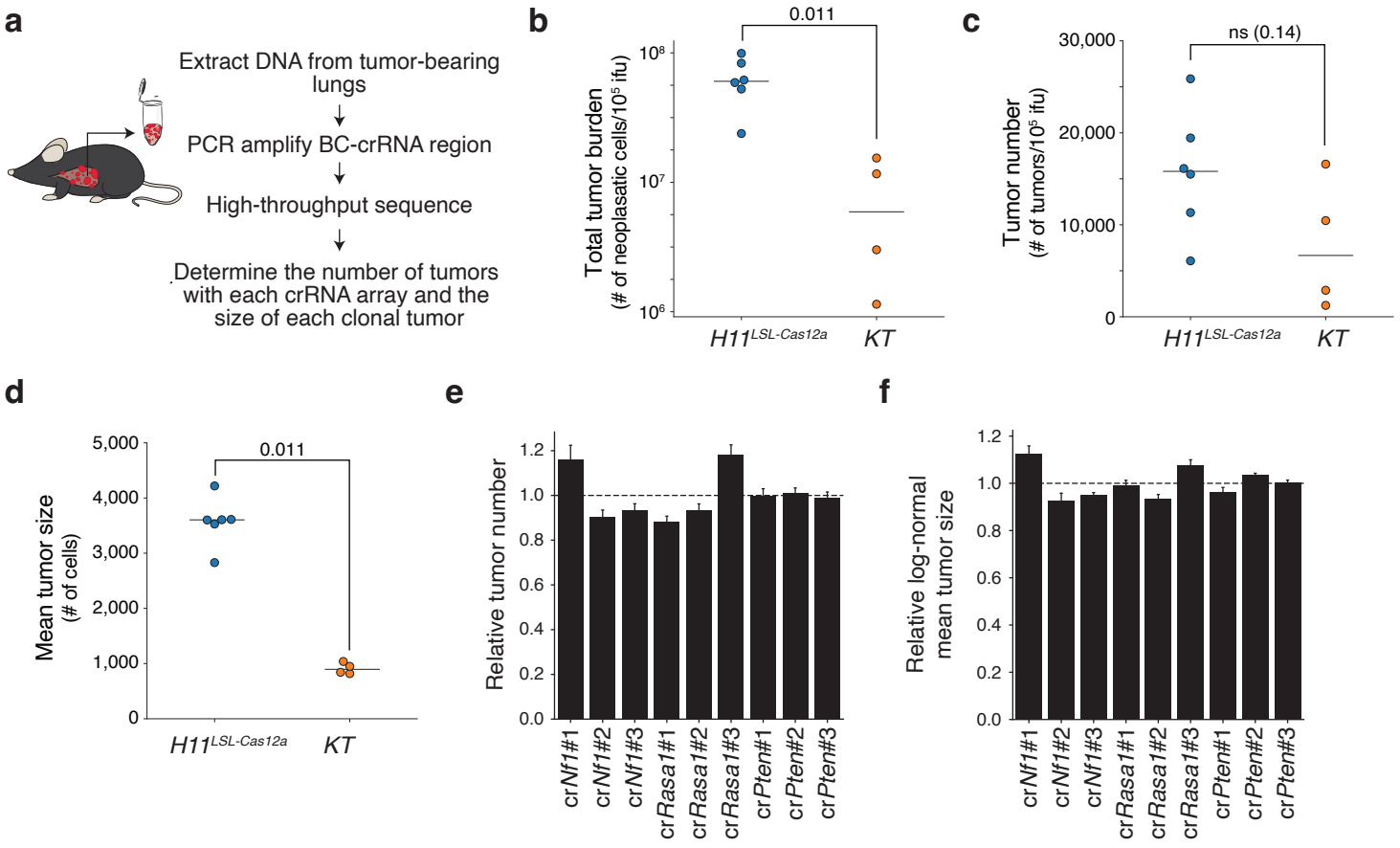

Figure 3. Integration of crRNA arrays with tumor barcoding enables quantification of tumor initiation and tumor size
a. Schematic of tumor barcoding with high-throughput BC-crRNA sequencing to determine the size of each Cas12a-induced clonal tumor.
b. Total number of neoplastic cells (Total tumor burden) in each mouse normalized to viral titer. Each dot represents a mouse, and bars are means. P-value calculated with Wilcoxon rank-sum test.
c. Number of tumors in each mouse normalized to viral titer. Each dot represents a mouse, and bars are means. P-value calculated with Wilcoxon rank-sum test.
d. Mean tumor size given a log-normal tumor size distribution. Each dot represents a mouse, and bars are means. P-value calculated with Wilcoxon rank-sum test.
e. Number of tumors for each crRNA (guide) relative to the median value for each gene. 95% confidence intervals are shown.
f. Mean tumor size assuming a log-normal distribution for each crRNA (guide) relative to the median value for each gene. 95% confidence intervals are shown.

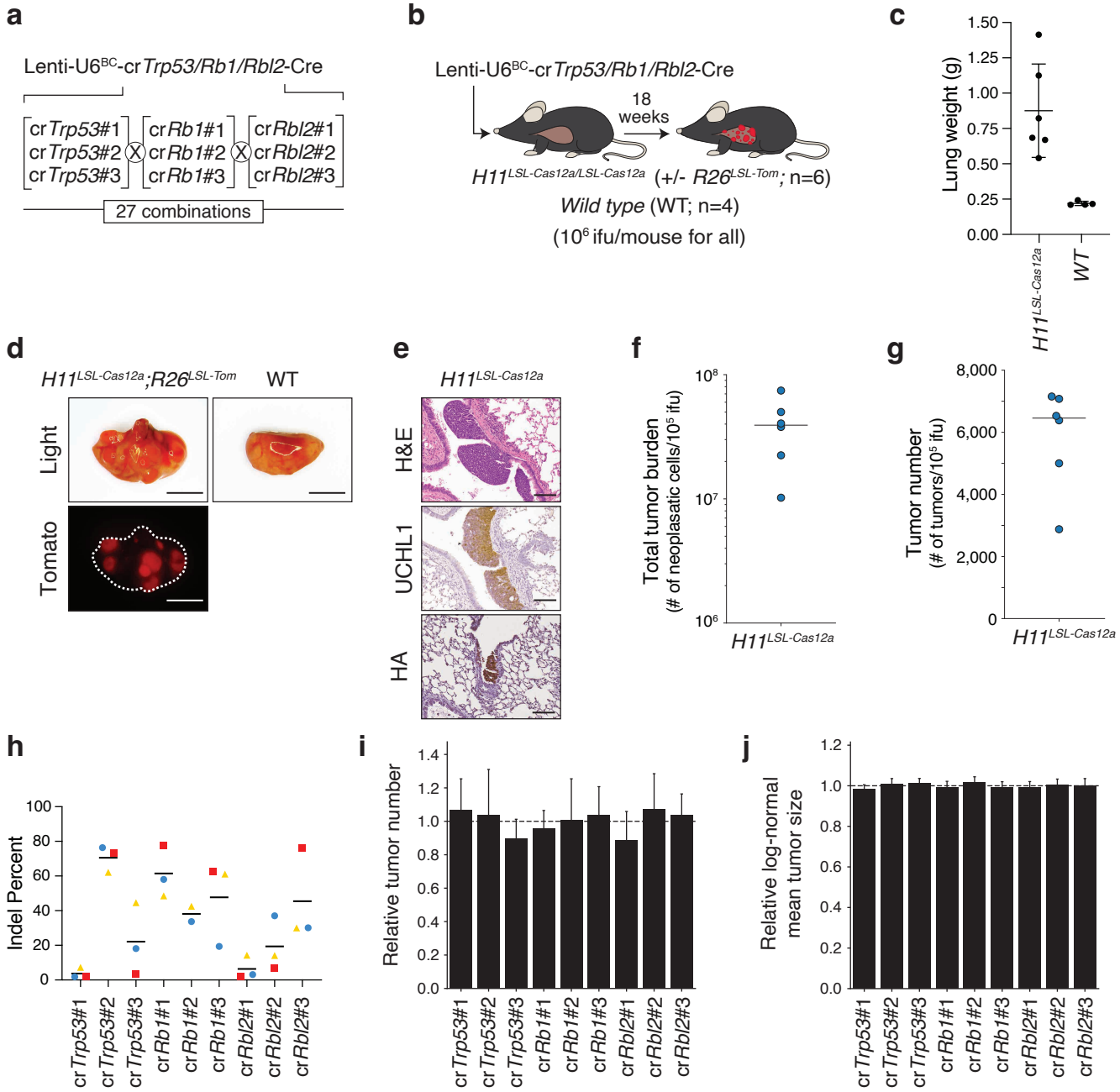

Figure 4. Induction of small-cell lung cancer through the simultaneous Cas12a-mediated inactivation of *Trp53, Rb1* and *Rbl2*

a. Lenti-U6^{BC}-cr*Trp53/Rb1/Rbl2*-Cre pool has guides targeting *Trp53, Rb1*, and *Rbl2*. Each gene is targeted by three crRNAs in all 27 combinations.

b. Intratracheal delivery of Lenti-U6^{BC}-cr*Trp53/Rb1/Rbl2*-Cre to *H11*$^{LSL\text{-}Cas12a}$ and *wild-type (WT)* mice. Viral titer (infectious units, ifu) and mouse numbers are indicated.

c. Lung weights from mice of the indicated genotypes 18 weeks after transduction with Lenti-U6^{BC}-cr*Trp53/Rb1/Rbl2*-Cre. Each dot represents a mouse. Mean +/- standard deviation is indicated.

d. Light (upper) and Tomato fluorescent (lower) images of lung lobes from the indicated genotypes of mice 18 weeks after transduction with Lenti-U6^{BC}-cr*Trp53/Rb1/Rbl2*-Cre. Dashed line outlines tissue. Tumors are Tomato-positive due to recombination of the *R26*$^{LSL\text{-}Tomato}$ allele. Scale bars, 5 mm.

e. Hematoxylin & eosin (upper), UCHL1 (middle) and HA tag (lower) staining of lung sections from an *H11*$^{LSL\text{-}Cas12a}$ mouse. Scale bars, 100 µm.

f. Total number of neoplastic cells (Total tumor burden) in each mouse normalized to viral titer. Each dot represents a mouse, and the bar is the mean.

g. The number of tumors in each mouse normalized to viral titer. Each dot represents a mouse, and the bar is the mean.

h. Indel frequencies for genomic regions targeted by each crRNA within micro-dissected tumor tissue from *H11*$^{LSL\text{-}Cas12a}$ mice. Symbol shapes and colors identify values from the same sample. Bars represent means.

i,j. Number of tumors (**i**) and mean tumor size assuming a log-normal distribution (**j**) for each crRNA (guide) relative to the median value for each gene. 95% confidence intervals are shown.

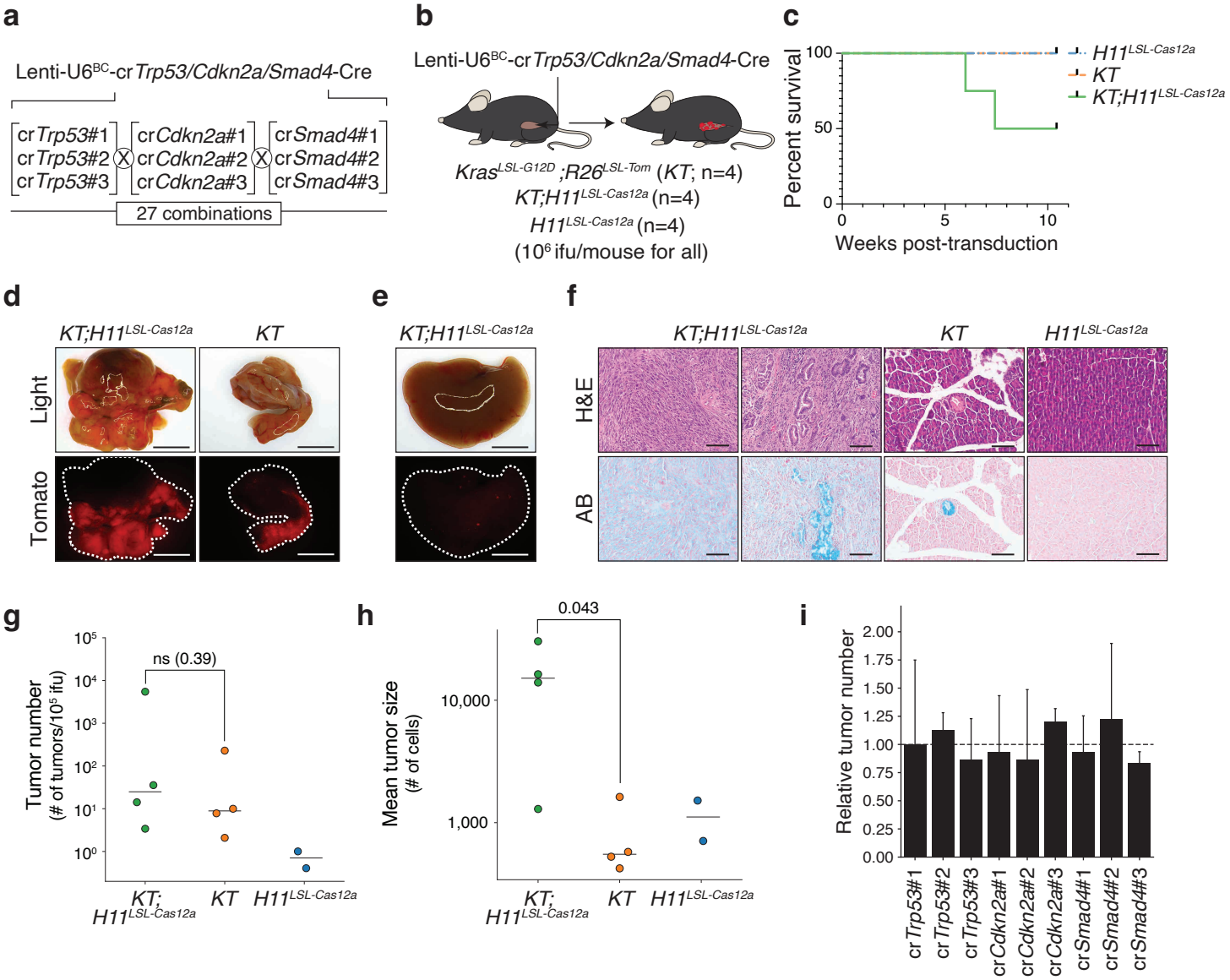

Figure 5. Rapid generation of PDAC through somatic Cas12a-mediated inactivation of commonly mutated tumor suppressor genes

a. Lenti-U6^{BC}-cr*Trp53/Cdkn2a/Smad4*-Cre pool has guides targeting *Trp53, Cdkn2a*, and *Smad4*. Each gene is targeted by three crRNAs in all 27 combinations.

b. Intrapancreatic delivery of Lenti-U6^{BC}-cr*Trp53/Cdkn2a/Smad4*-Cre to *Kras$^{LSL-G12D}$;R26$^{LSL-Tom}$* (*KT*), *KT;H11$^{LSL-Cas12a}$*, and *H11$^{LSL-Cas12a}$* mice. Viral titer (infectious units, ifu) and mouse numbers are indicated.

c. Survival curve of mice of the indicated genotypes transduced with Lenti-U6^{BC}-cr*Trp53/Cdkn2a/Smad4*-Cre.

d. Light (upper) and fluorescent Tomato (lower) pancreas images from the indicated genotypes of mice 6 weeks (*KT;H11$^{LSL-Cas12a}$*) or 11 weeks (*KT*) after transduction with Lenti-U6^{BC}-cr*Trp53/Cdkn2a/Smad4*-Cre. Dashed lines outline tissues. Scale bars, 5 mm.

e. Light and fluorescent Tomato images of a liver lobe from a *KT;H11$^{LSL-Cas12a}$* mouse. Dashed line outlines tissue. Scale bars, 5 mm.

f. Immunohistochemistry images of pancreas sections from the indicated genotypes, showing hematoxylin & eosin (H&E; upper) and Alcian Blue (AB; lower) staining. *KT;H11$^{LSL-Cas12a}$* panels show representative regions with poorly differentiated sarcomatoid carcinoma (left; approximately 80-90% of tumor area) and more differentiated areas with mucinous cells and some lobular structure (right). Scale bars, 100 µm.

g. The number of tumors in each mouse normalized to viral titer. Each dot represents a mouse, and bars are means. Note that two *H11$^{LSL-Cas12a}$* mice did not have detectable tumor burden and are not plotted. P-value calculated with Wilcoxon rank-sum test.

h. Mean tumor size given a log-normal tumor size distribution. Each dot represents a mouse, and bars are means. Note that two *H11$^{LSL-Cas12a}$* mice did not have detectable tumor burden and are not plotted. P-value calculated with Wilcoxon rank-sum test.

i. Number of tumors for each crRNA (guide) relative to the median value for each gene. 95% confidence intervals are shown.

a

	Cas9	Cas12a
Structural features		
RNA scaffold	tracrRNA (~100 nt/guide)	Direct repeats (DR;~20 nt each)
Promoter	one per sgRNA	one per crRNA array
Cloning	one step per sgRNA	one step per crRNA array
Guide uncoupling due to lentiviral template switching	high	low
Ability to sequence across 3 guides	difficult	easy
Cutting		
Cut site relative to PAM	3 bp from PAM	18 bp from the PAM
Cuts	blunt-end	5 nt staggered

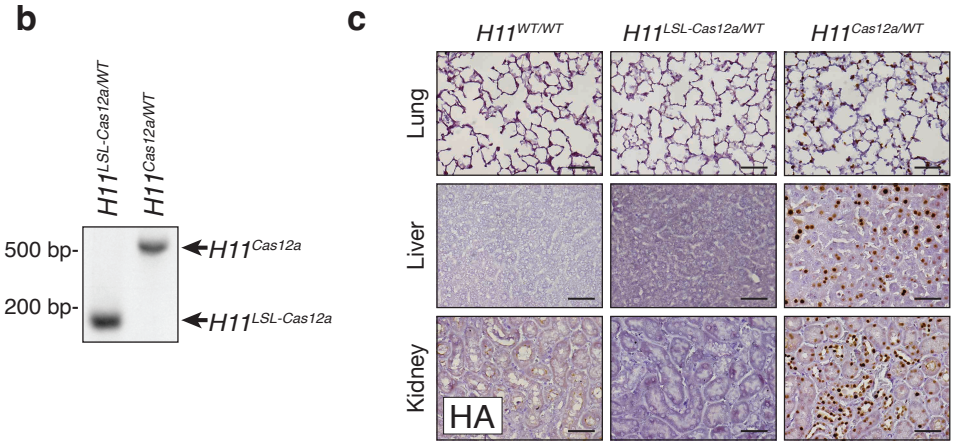

Supplementary Figure 1. Comparison of salient features of Cas9 and Cas12a, and broad nuclear expression of Cas12a in *H11*^{Cas12a} mice

a. Summary of features of Cas9 and Cas12a relevant to multiplexed genome editing. Note that the potential impact of off-target effects is increased when targeting more genes.

b. PCR genotyping of mice of the indicated *H11*$^{LSL\text{-}Cas12a}$ and *H11*^{Cas12a} genotypes.

c. Immunohistochemical staining for the Cas12a HA tag in lung, liver and kidney sections from the indicated genotypes of mice. Scale bars, 50 μm. Higher magnification images of these liver sections is shown in Figure 1f.

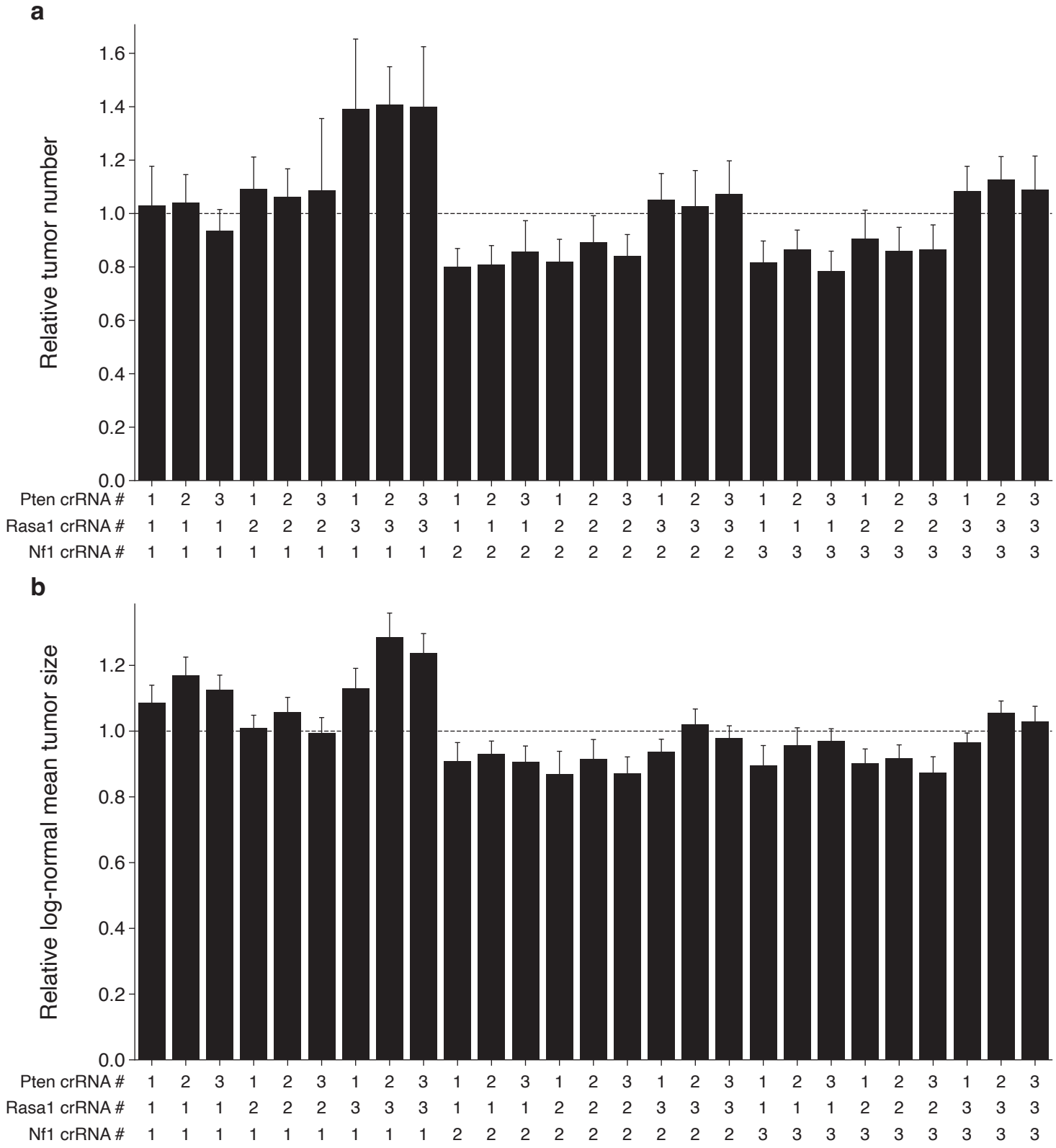

Supplementary Figure 2. Incorporation of Cas12a-mediated genome editing with Tuba-seq^{Ultra} enables quanitification of the effects of each crRNA array

a,b. Number of tumors (**a**) and mean tumor size assuming a log-normal distribution (**b**) for each crRNA array (27 combinations in total) relative to the median value for all arrays in *H11*$^{LSL\text{-}Cas12a}$ mice. 95% confidence intervals are shown.

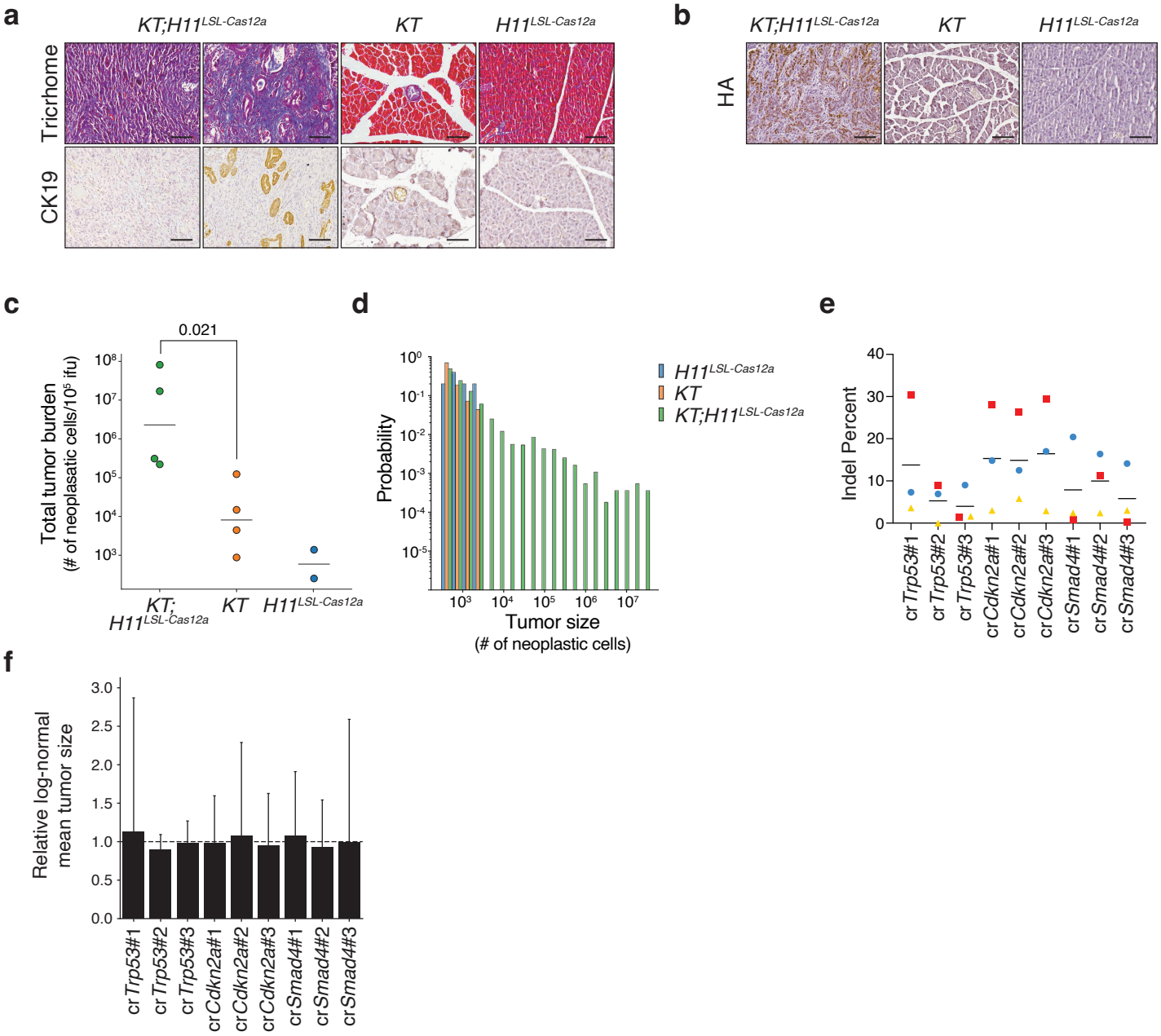

Supplementary Figure 3. Inactivation of *Trp53*, *Cdkn2a*, and *Smad4* greatly increases tumor size and leads to the development of PDAC with differentiated areas with CK19+ cancer cells and desmoplastic stroma as well as more poorly differentiated areas

a. Immunohistochemistry images of pancreas sections from the indicated genotypes, showing Trichrome (upper) and Cytokeratin-19 (CK19; lower) staining. *KT;H11*$^{LSL\text{-}Cas12a}$ panels show representative poorly differentiated (left) and more differentiated (right) regions. Scale bars, 100 µm.

b. Immunohistochemical staining for the Cas12a HA tag on pancreas tissue from representative *KT;H11*$^{LSL\text{-}Cas12a}$, *KT* and *H11*$^{LSL\text{-}Cas12a}$ mice transduced with Lenti-U6^{BC}-cr*Trp53/Cdkn2a/Smad4*-Cre. Scale bars, 100 µm.

c. Total number of neoplastic cells (Total tumor burden) in each mouse normalized to viral titer. Each dot represents a mouse and the bar is the mean. Note that two *H11*$^{LSL\text{-}Cas12a}$ mice did not have detectable tumor burden and are not plotted. P-value calculated with Wilcoxon rank-sum test.

d. Probability distribution of the size of tumors in the indicated genotypes of mice.

e. Indel frequencies for genomic regions targeted by each crRNA within bulk tumor-bearing pancreas tissue from KT;*H11*$^{LSL\text{-}Cas12a}$ mice. Tissue samples had variable tumor burden, likely explaining observed variability in indel frequencies. Symbol shapes and colors identify values from the same mouse. Bars represent means.

f. Mean tumor size assuming a log-normal distribution for each crRNA (guide) relative to the median value for each gene. 95% confidence intervals are shown.

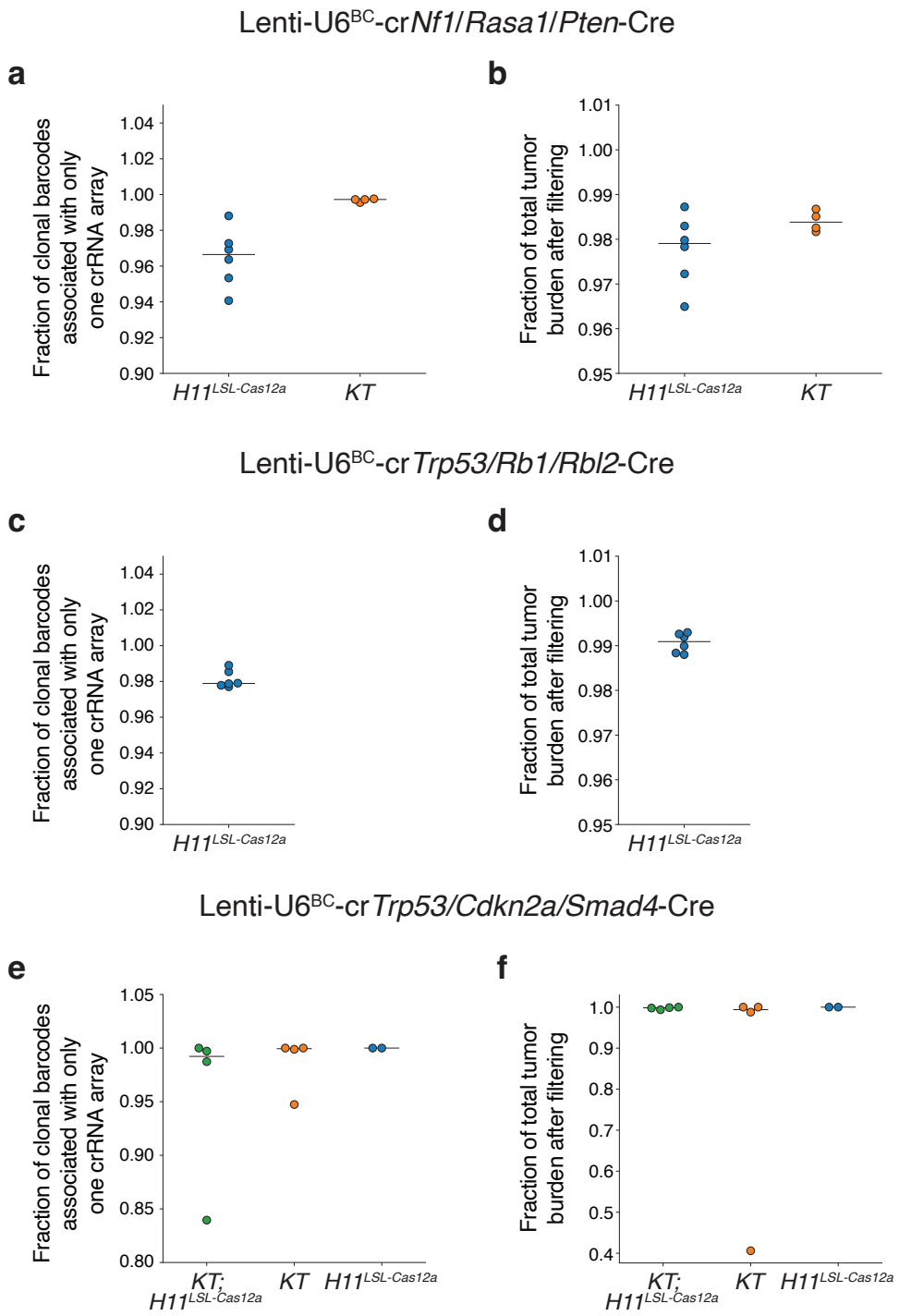

Supplementary Figure 4. Generation of Cas12a Lenti-U6^{BC}-crRNA-Cre vector libraries is associated with minimal shuffling of crRNA sequences

a,c,e. Fraction of all U6-integrated barcode reads that are associated with only a single crRNA array within each vector pool in the indicated mouse genotypes: Lenti-U6^{BC}-cr*Nf1*/*Rasa1*/*Pten*-Cre (**a**), Lenti-U6^{BC}-cr*Trp53/Rb1/Rbl2*-Cre (**c**), and Lenti-U6^{BC}-cr*Trp53/Cdkn2a/Smad4*-Cre (**e**). Bars represent medians.

b,d,f. Fraction of total neoplastic cells (total tumor burden) remaining after filtering out spurious "tumor" reads arising during library preparation and sequencing of each pool in the indicated mouse genotypes: Lenti-U6^{BC}-cr*Nf1*/*Rasa1*/*Pten*-Cre (**b**), Lenti-U6^{BC}-cr*Trp53/Rb1/Rbl2*-Cre (**d**), and Lenti-U6^{BC}-cr*Trp53/Cdkn2a/Smad4*-Cre (**f**). Bars represent medians.